Biophysical Chemistry 162 (2012) 45–60

Contents lists available at SciVerse ScienceDirect

Biophysical Chemistry

journal homepage: http://www.elsevier.com/locate/biophyschem

Simulation of NO and O_2 transport facilitated by polymerized hemoglobin solutions in an arteriole that takes into account wall shear stress-induced NO production

Yipin Zhou [a], Pedro Cabrales [b], Andre F. Palmer [a,*]

[a] William G. Lowrie Department of Chemical and Biomolecular Engineering, The Ohio State University, Columbus, OH 43210, USA
[b] Department of Bioengineering, University of California, San Diego, La Jolla, CA 92093, USA

HIGHLIGHTS

- Developed mathematical model of nitric oxide and oxygen transport in an arteriole.
- Arteriole contained a mixture of red blood cells and HBOCs.
- Model accounted for wall shear stress-induced production of nitric oxide.

GRAPHICAL ABSTRACT

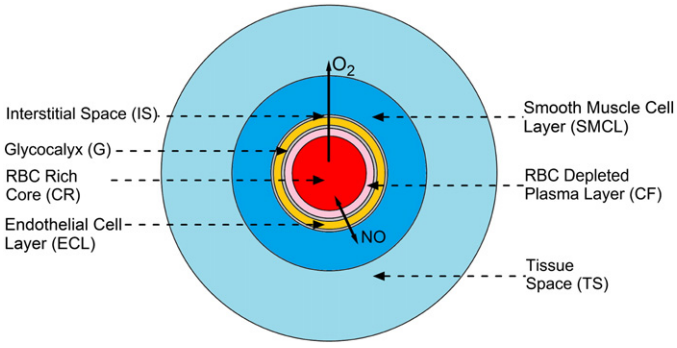

ARTICLE INFO

Article history:
Received 21 November 2011
Received in revised form 20 December 2011
Accepted 20 December 2011
Available online 9 January 2012

Keywords:
Mathematical model
Blood substitute
Hemoglobin-based oxygen carrier
Polymerized bovine hemoglobin
Oxygen transport
Nitric oxide transport

ABSTRACT

A mathematical model was developed to study nitric oxide (NO) and oxygen (O_2) transport in an arteriole and surrounding tissues exposed to a mixture of red blood cells (RBCs) and hemoglobin (Hb)-based O_2 carriers (HBOCs). A unique feature of this model is the inclusion of blood vessel wall shear stress-induced production of endothelial-derived NO, which is very sensitive to the viscosity of the RBC and HBOC mixture traversing the blood vessel lumen. Therefore in this study, a series of polymerized bovine Hb (PolyHb) solutions with high viscosity, varying O_2 affinities, NO dioxygenation rate constants and O_2 dissociation rate constants that were previously synthesized and characterized by our group was evaluated via mathematical modeling, in order to investigate the effect of these biophysical properties on the transport of NO and O_2 in an arteriole and its surrounding tissues subjected to anemia with the commercial HBOC Oxyglobin® and cell-free bovine Hb (bHb) serving as appropriate controls. The computer simulation results indicated that transfusion of high viscosity PolyHb solutions promoted blood vessel wall shear stress dependent generation of the vasodilator NO, especially in the blood vessel wall and should transport enough NO inside the smooth muscle layer to activate vasodilation compared to the commercial HBOC Oxyglobin® and cell-free bHb. However, NO scavenging in the arteriole lumen was unavoidable due to the intrinsic high NO dioxygenation rate constant of the HBOCs being studied. This study also observed that all PolyHbs could potentially improve tissue oxygenation under hypoxic conditions, while low O_2 affinity PolyHbs were more effective in oxygenating tissues under normoxic conditions compared with high O_2 affinity PolyHbs. In addition, all ultrahigh molecular weight PolyHbs displayed higher O_2 transfer rates than the commercial HBOC Oxyglobin® and cell-free bHb. Therefore, these results suggest that ultrahigh molecular weight PolyHb solutions could be used as safe and efficacious O_2 carriers for use in transfusion medicine. It also suggests that future generations of PolyHb solutions should possess lower NO dioxygenation reaction rate constants in order to reduce NO scavenging,

* Corresponding author. Tel.: +1 614 292 6033.
E-mail addresses: stephen1760@gmail.com (Y. Zhou), pcabrales@ucsd.edu (P. Cabrales), palmer.351@osu.edu (A.F. Palmer).

0301-4622/$ – see front matter
doi:10.1016/j.bpc.2011.12.006

while maintaining high solution viscosity to take advantage of wall shear stress-induced NO production. Taken together, we suggest that this mathematical model can be used to predict the vasoactivity of HBOCs and help guide the design and optimization of the next generation of HBOCs for use in transfusion medicine.

1. Introduction

Hemoglobin (Hb)-based oxygen (O_2) carriers (HBOCs) have been under development as a universal readily-available O_2 carrying solution to be used in transfusion medicine for patients suffering from moderate to serve anemia [1–5]. Despite significant commercial development, only the polymerized bovine Hb (bHb) product Hemopure® (HBOC-201, OPK Biotech, Cambridge, MA) is approved for clinical use in South Africa [6]. Recent late stage clinical results showed that HBOCs elicit vasoconstriction in the microcirculation and lead to the development of systemic hypertension [7–10]. One possible reason for the occurrence of Hb-induced vasoconstriction stems from the rapid scavenging of the vasodilatory molecule nitric oxide (NO) by cell-free Hb in the circulation [11,12].

NO is an important messenger molecule *in vivo*, which plays important roles in many physiological processes such as regulation of cellular respiration [13,14] and vascular tone [15], induction of angiogenesis [16,17], enhancement of wound healing [18,19], and facilitation of nervous system signaling [20]. NO is mainly generated by the layer of endothelial cells that comprise the blood vessel wall via both enzymatic and non-enzymatic pathways [21–23]. When NO diffuses into the smooth muscle cell layer of the blood vessel wall, NO can activate soluble guanylate cyclase (sGC) [21] which converts guanosine triphosphate (GTP) into 3′,5′-cyclic guanosine monophosphate (cGMP) [24] and induces the relaxation (*i.e.* dilation) of the blood vessel. When it diffuses into blood, NO can react rapidly with heme-containing macromolecules such as acellular cell-free Hb and HBOCs [25] forming nitrate and methemoglobin (metHb). Thus, cell-free Hb and HBOCs are usually considered as NO sinks [26]. To further complicate matters, αβ dimers, tetrameric Hb and small polymerized Hb molecules can extravasate out of the blood vessel lumen through pores in the blood vessel wall, where these molecules can scavenge NO thereby eliciting vasoconstriction and systemic hypertension [26], which is one of the main side-effects hampering the clinical use of currently commercially available HBOCs [7–10,18].

The bioavailability of NO derived from the endothelial cell layer can be influenced by various extracellular factors such as the shear stress acting on the blood vessel wall and various oxidative stresses [12,27]. Both experimental studies on *in vitro* cell cultures and animal models, as well as, mathematical simulations have observed and predicted that increasing the wall shear stress on the endothelium can increase the production rate of NO [28–33]. In the physiological range of observed blood vessel wall shear stresses ranging from 6 to 25 dyn/cm^2, the rate of release of NO was found to be linearly dependent on the shear stress acting on the blood vessel wall [34,35]. To further emphasize the importance of shear stress-induced NO production, Cabrales et al. reported that transfusion of high viscosity > 500 kDa fraction of ultrahigh molecular weight (MW) glutaraldehyde polymerized bHb (PolyHb) solutions synthesized by our group [36,37] elicited little to no vasoconstriction in a hamster top-load model [38] and in an exchange transfusion model [39], while the commercial low MW polymerized HBOC Oxyglobin® (average MW ~200 kDa) elicited severe hypertension [40], although these various PolyHbs possessed NO dioxygenation rate constants that were similar to that of cell-free Hb. Compared to Oxyglobin® (1.8 cP at a total Hb concentration of 13 g/dL) [39], the viscosities of PolyHbs synthesized by our group are much higher than that of Oxyglobin® (3.6–14 cP at a total Hb concentration of 10 g/dL). Thus, it is reasonable to hypothesize that high viscosity PolyHb solutions should be able to enhance shear stress-induced production of NO, which should offset the rapid NO scavenging ability of acellular HBOCs.

Therefore, investigating simultaneous NO and O_2 transport in the presence of PolyHb solutions, especially accounting for blood vessel wall shear stress-induced production of NO due to transfused HBOCs, can be beneficial in understanding and evaluating the potential efficacy and safety of PolyHb solutions upon transfusion and optimize their future design in order to mitigate the harmful vasoconstrictive and hypertensive effects. In a previous study by our group, a NO/O_2 transport model was developed in order to investigate NO/O_2 transport in an arteriole and its surrounding tissues facilitated by various types of HBOCs [41]. However, shear stress-induced generation of endothelial-derived NO was not taken into account, which in turn may underestimate NO production upon transfusion of HBOC solutions. In addition, to our knowledge, a mathematical model of simultaneous NO/O_2 transport *in vivo* facilitated by ultra-high MW PolyHbs has never been conducted to date. We hypothesize that PolyHb formulations with high solution viscosity and that correspondingly yield high blood vessel wall shear stresses should help to facilitate an increase in tissue oxygenation upon transfusion, while maintaining adequate NO levels in the smooth muscle layer to induce vasodilation.

More specifically in this study, we propose to develop an improved NO and O_2 transport model in a hamster arteriole exposed to a mixture of hemodiluted RBCs (to simulate the anemic state) and PolyHbs in order to investigate the effect of blood vessel wall shear stress-induced NO production caused by transfusion of highly viscous PolyHb solutions on NO transport and O_2 transport in an arteriole and its surrounding tissues upon transfusion of various PolyHb solutions having different biophysical properties such as MW, diffusivity, O_2 affinity, O_2 dissociation kinetics and NO dioxygenation rate constant. The commercially available polymerized HBOC product Oxyglobin® and acellular bHb will be simulated for comparison.

2. Materials and methods

2.1. Computational methods

A mathematical model based on modification of the Krogh tissue cylinder (KTC) model [41,42] was used to simulate mass transport of NO and O_2 in a single arteriole to the surrounding tissues upon transfusion of PolyHb solutions (Fig. 1). The geometry of the arteriole and the surrounding tissue region was subdivided into 7 regions: 1) the RBC-rich core ($0 \le r \le r_1$); 2) the RBC-poor plasma layer ($r_1 < r \le r_2$); 3) a stagnant protein glycocalyx layer (G) ($r_2 < r \le r_3$); 4) the endothelial cell layer (E) ($r_3 < r \le r_4$); 5) the cell-free interstitial space (IS) ($r_4 < r \le r_5$); 6) the smooth muscle cell layer (SMC) ($r_5 < r \le r_6$) and 7) the tissue space (TS) ($r_6 < r \le r_7$) (Fig. 1.B). The arteriole was assigned a length (L_c) of 500 μm and a diameter of 60 μm (Fig. 1.A). In this model, RBCs and PolyHb molecules flow through the arteriolar region ($0 \le r \le r_2$) and enter the arteriole at $Z = 0$ and exit it at $Z = L_c$. O_2 is assumed to be transported by the convective flow of dissolved O_2, oxygenated RBCs and PolyHbs as well as other HBOCs in the blood. Due to the presence of the O_2 gradient originating from the blood to the tissue space, O_2 diffuses through the blood vessel wall into the endothelial cell layer, smooth muscle layer and tissue space where it is consumed, while NO is generated only by the endothelial cell layer and diffuses into both the blood compartment and surrounding smooth muscle cell layer and tissue. The extravasation of PolyHb molecules through the blood vessel wall,

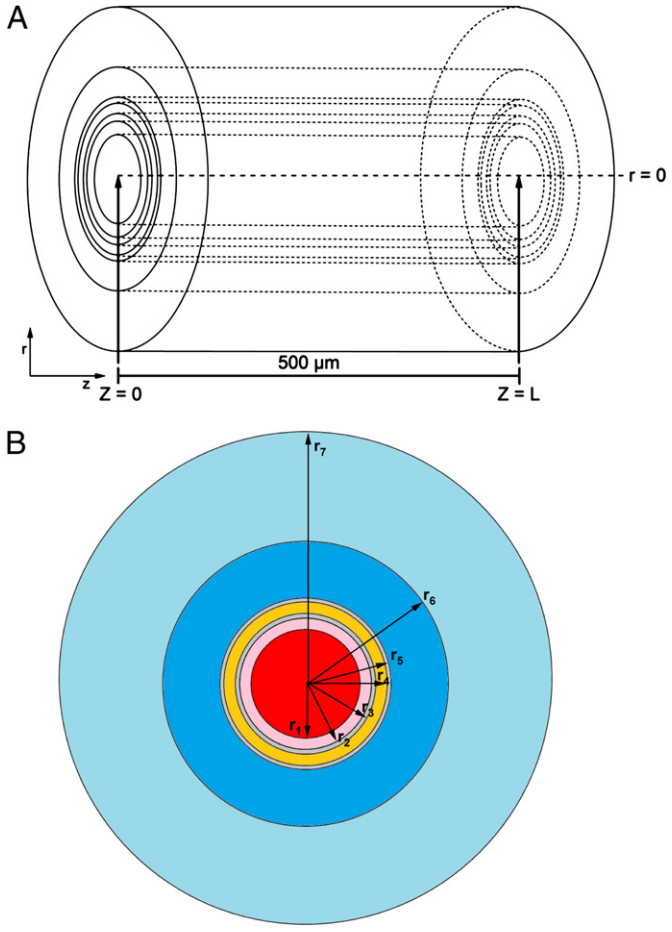

Fig. 1. Model geometry of an arteriole. A: Side-view of the 500 μm long arteriole and surrounding tissue used in the simulation. B: Schematic cross-section of the modified KTC model geometry delineating each subregion: 1) RBC-rich core ($0 \le r \le r_1$); 2) RBC-poor plasma layer ($r_1 < r \le r_2$); 3) stagnant protein glycocalyx layer (G) ($r_2 < r \le r_3$); 4) endothelial cell layer (E) ($r_3 < r \le r_4$); 5) cell-free interstitial space (IS) ($r_4 < r \le r_5$); 6) smooth muscle cell layer (SMC) ($r_5 < r \le r_6$) and 7) tissue space (TS) ($r_6 < r \le r_7$). r: radius; *Z*, axial coordinate.

vasoconstriction and change of blood flow rate following transfusion of the HBOCs was not considered in this model. This mathematical model was numerically simulated using the Chemical Engineering module of COMSOL Multiphysics software (Comsol, Burlington, MA).

2.2. Hb-O_2 release/binding kinetics

The kinetics of gaseous ligand binding and release between dissolved O_2 and Hb inside RBCs/HBOCs is reversible and can be derived from a simplified reaction between one O_2 molecule and one heme group (Eq. (1)) of the Hb tetramer. Thus, all calculations in this chapter will be based on the amount of heme groups present in RBCs and HBOCs (Eq. (2)). The total amount of Hb is represented by the sum of oxygenated Hb (HbO_2, oxyHb) and deoxygenated Hb (Hb, deoxyHb) (Eq. (3)), and the fractional saturation of Hb with O_2 is defined as *S* (Eq. (4)). The rate of formation of O_2 from HbO_2 (R_{O2}) is described by Eq. (5), where $k_{off,O2}$ and $k_{on,O2}$ are the O_2 dissociation and association rate constants of Hb, respectively. At equilibrium, when R_{O2} is equal to zero, $k_{on,O2}$ is given by Eq. (6), where Y_e is the fractional saturation of Hb with O_2 at equilibrium. Y_e was calculated using a 4-step Adair model [43] (Eq. (7)), which is more accurate than the one-step Hill model [44] in order to increase the physiological relevance of the simulation [45], where a_1–a_4 represent the Adair constants for either RBCs or HBOCs (listed in Table 3). After reorganizing the equations, the expression for R_{O2} can be rewritten in the form of Eq. (8). Therefore, the corresponding rates of formation of O_2 from releasing of O_2 from HbO_2 contained inside RBCs and HBOCs are given as Eqs. (9) and (10), respectively.

The rate of formation of HbO_2 is given by the following equation $R_{HbO2} = -R_{O2}$. The rate of formation of HbO_2 in RBCs and HBOCs is described by Eqs. (11) and (12), respectively.

$$O_2 + Hb \underset{k_{off,O2}}{\overset{k_{on,O2}}{\rightleftharpoons}} HbO_2 \tag{1}$$

$$[Heme]_{HBOC} = \frac{[HBOC]_{overall}}{MW_{HBOC}} \cdot \frac{MW_{HBOC}}{MW_{bHb}} \cdot 4 = \frac{4 \cdot [HBOC]_{overall}}{MW_{bHb}} \tag{2}$$

$$[Hb]_{total} = [Hb] + [HbO_2] \tag{3}$$

$$S = \frac{[HbO_2]}{[Hb]_{total}} \tag{4}$$

$$R_{O2} = k_{off,O2} \cdot [HbO_2] - k_{on,O2} \cdot [O_2] \cdot [Hb] \tag{5}$$

$$k_{on,O2} = \frac{k_{off,O2} \cdot Y_e}{[O2] \cdot (1 - Y_e)} \tag{6}$$

$$Y_e = \frac{a_1 \cdot pO_2 + 2a_2 \cdot pO_2^{\,2} + 3a_3 \cdot pO_2^{\,3} + 4a_4 \cdot pO_2^{\,4}}{4(1 + a_1 \cdot pO_2 + a_2 \cdot pO_2^{\,2} + a_3 \cdot pO_2^{\,3} + a_4 \cdot pO_2^{\,4})} \tag{7}$$

$$\begin{aligned} R_{O2} &= k_{off,O2} \cdot [Hb]_{total} \cdot S - \frac{k_{off,O2} \cdot Y_e}{(1 - Y_e)} \cdot [Hb]_{total} \cdot (1 - S) \\ &= k_{off,O2} \cdot [Hb]_{total} \cdot \left[S - \frac{Y_e}{1 - Y_e} \cdot (1 - S) \right] \end{aligned} \tag{8}$$

$$R_{O2,RBC} = k_{off,O2\text{-}RBC} \cdot [Hb_{RBC}]_{total} \cdot \left[S_{RBC} - \frac{Y_{e,RBC}}{1 - Y_{e,RBC}} \cdot (1 - S_{RBC}) \right] \tag{9}$$

$$R_{O2,HBOC} = k_{off,O2\text{-}HBOC} \cdot [HBOC]_{total} \cdot \left[S_{HBOC} - \frac{Y_{e,HBOC}}{1 - Y_{e,HBOC}} \cdot (1 - S_{HBOC}) \right] \tag{10}$$

$$R_{HbO2\text{-}RBC} = k_{off,O2\text{-}RBC} \cdot [Hb_{RBC}]_{total} \cdot \left[\frac{Y_{e,RBC}}{1 - Y_{e,RBC}} \cdot (1 - S_{RBC}) - S_{RBC} \right] \tag{11}$$

$$R_{HbO2\text{-}HBOC} = k_{off,O2\text{-}HBOC} \cdot [HBOC]_{total} \cdot \left[\frac{Y_{e,HBOC}}{1 - Y_{e,HBOC}} \cdot (1 - S_{HBOC}) - S_{HBOC} \right] \tag{12}$$

3. Mass balance on O_2/NO with Hb encapsulated within RBCs and HBOCs

3.1. Arteriole lumen ($0 \le r \le r_2$)

In the arteriole lumen, blood can be roughly considered as a solution of RBCs. The RBC concentration can be described as a function of the hematocrit (*hct*), which is the percentage of the total blood volume occupied by packed RBCs [46]. However, due to the Fåhraeus effect, RBCs tend to migrate toward the central axis of the blood vessel, which generates a RBC-rich core with higher Hb concentration and a RBC-poor plasma region with correspondingly lower Hb concentration [47,48]. In the RBC-rich core, the local *hct* is higher than the discharge *hct* (H_D) and is assumed to be a constant value (H_C), while in the RBC-poor plasma region, the *hct* decreases from the core region toward the blood vessel wall and can be described by different concentration profiles ranging from step, linear and parabolic profiles [32,49]. Chen et al. [49] investigated the effect of these

three *hct* profiles on NO/O_2 transport by mathematical modeling and observed that the simulation results obtained by using a linear profile to describe the *hct* in the RBC-poor region were in good agreement with experimental data. Thus, in this chapter, a linear *hct* profile and blood velocity (v_z) profile (Fig. 2) will be used to define the local blood velocity and *hct* at a given radius (r) (Eqs. (13) and (14) where U_{avg} is the average blood velocity). H_C will be calculated by performing a mass balance on RBCs in the arteriole lumen (Eq. (15)). Thus, the local concentration of Hb that is derived from RBCs is given by Eq. (16), while the luminal HBOC concentration will be determined by Eq. (17).

$$hct(\mathrm{r}) = \begin{cases} H_c & 0<\mathrm{r}\le \mathrm{r}_1 \\ H_c \cdot \dfrac{\mathrm{r}_2-\mathrm{r}}{\mathrm{r}_2-\mathrm{r}_1} & \mathrm{r}_1<\mathrm{r}\le \mathrm{r}_2 \end{cases} \tag{13}$$

$$v_z = \begin{cases} U_{avg} & 0<\mathrm{r}\le \mathrm{r}_1 \\ U_{avg} \cdot \dfrac{\mathrm{r}_2-\mathrm{r}}{\mathrm{r}_2-\mathrm{r}_1} & \mathrm{r}_1<\mathrm{r}\le \mathrm{r}_2 \end{cases} \tag{14}$$

$$2\pi \cdot \int_0^{\mathrm{r}_2} hct(\mathrm{r}) \cdot v_z \cdot \mathrm{r}d\mathrm{r} = 2\pi \cdot H_D \cdot \int_0^{\mathrm{r}_2} v_z \cdot \mathrm{r}d\mathrm{r} \tag{15}$$

$$[\mathrm{Hb}_{RBC}]_{\mathrm{total}} = [\mathrm{Hb}]_{RBC\text{-}overall} \cdot hct \tag{16}$$

$$[\mathrm{HBOC}]_{\mathrm{total}} = [\mathrm{HBOC}]_{\mathrm{overall}} \cdot \frac{1-hct}{1-H_D} \tag{17}$$

O_2 in the arteriole lumen will be transported by stead-state convection and diffusion in the plasma and will reversibly bind to heme groups in RBCs and HBOCs. Thus, the mass balance for the formation of O_2 inside the lumen is described by Eq. (18), where α is the solubility of O_2 in aqueous media, D_{O2} is the diffusivity of O_2. $z' = \left(\frac{z}{L_c}\right)$ is the dimensionless length and $\mathrm{r}' = \left(\frac{\mathrm{r}}{R_c}\right)$ is the dimensionless radius. $\left[\mathrm{pO_2}\right]' = \left(\frac{\mathrm{pO_2}}{P_{50\text{-}RBC}}\right)$ is the dimensionless local O_2 partial pressure, where $P_{50\text{-RBC}}$ is the P_{50} of RBCs and $v_z' = \left(\frac{v_z}{U_{avg}}\right)$ is the dimensionless blood velocity. Similarly, mass balances of luminal RBCs and HBOCs are given by Eqs. (19) and (20), in which $D_{Hb\text{-}RBC}$ and D_{HBOC} represent the diffusivity of Hb inside RBCs and diffusivity of HBOC molecules in plasma, respectively; and $k_{off,O2\text{-}RBC}$ and $k_{off,O2\text{-}HBOC}$ represent the O_2 dissociation rate constants of RBCs and HBOCs, respectively. On the other hand, NO is transported via steady-state convection and diffusion but scavenged by Hb encapsulated in RBCs and HBOCs via a first-order reaction (*i.e.* NO dioxygenation reaction represented by Eq. (21)) where $k_{ox,NO\text{-}RBC}$ and $k_{ox,NO\text{-}HBOC}$ represent the NO dioxygenation rate constants of RBCs and HBOCs, respectively. Therefore, the mass balance on NO is shown in Eqs. (22) and (23), where $\left[\mathrm{NO}\right]' = \frac{[\mathrm{NO}]}{[\mathrm{NO}^0]}$ is the dimensionless NO concentration, D_{NO} is the diffusivity of NO and $[\mathrm{NO}^0]$ is the basal NO concentration and R_{NO} is the dioxygenation rate constant of NO with oxyHb in RBCs and HBOCs. In this work, the oxidation reaction between NO and O_2 is neglected due to the low reaction rate in comparison to the reaction rate of the NO dioxygenation reaction [50].

$$\begin{aligned} \frac{\alpha \cdot U_{avg} \cdot P_{50\text{-}RBC} \cdot v_z'}{L_c} \cdot \frac{\partial \mathrm{O}_2}{\partial z'} &= \alpha \cdot DO_2 \cdot P_{50} \cdot \left[\nabla'^2 \left[\mathrm{pO_2}\right]'\right] \\ &+ k_{off,O2\text{-}RBC} \cdot [\mathrm{Hb}_{RBC}]_{\mathrm{total}} \cdot \left[S_{RBC} - \frac{Y_{e,RBC}}{1-Y_{e,RBC}} \cdot (1-S_{RBC})\right] \\ &+ k_{off,O2\text{-}HBOC} \cdot [\mathrm{HBOC}]_{\mathrm{total}} \cdot \left[S_{RBC} - \frac{Y_e}{1-Y_e} \cdot (1-S_{RBC})\right] \end{aligned} \tag{18}$$

$$\begin{aligned} \frac{U_{avg}}{L_c} \cdot v'_z \cdot \frac{\partial S_{RBC}}{\partial z} &= D_{Hb\text{-}RBC} \cdot \left[\nabla^2 S_{RBC}\right] \\ &+ k_{off,O2\text{-}RBC} \cdot \left[\frac{Y_{e,RBC}}{1-Y_{e,RBC}} \cdot (1-S_{RBC}) - S_{RBC}\right] \end{aligned} \tag{19}$$

$$\begin{aligned} \frac{U_{avg}}{L_c} \cdot v'_z \cdot \frac{\partial S_{HBOC}}{\partial z} &= D_{HBOC} \cdot \left[\nabla^2 S_{HBOC}\right] \\ &+ k_{off,O2\text{-}HBOC} \cdot \left[\frac{Y_{e,HBOC}}{1-Y_{e,HBOC}} \cdot (1-S_{HBOC}) - S_{HBOC}\right] \end{aligned} \tag{20}$$

$$\mathrm{Hb} + \mathrm{NO} \xrightarrow{kox\text{-}NO} \mathrm{HbNO} \tag{21}$$

$$\frac{U_{avg} \cdot \left[\mathrm{NO}^0\right]}{L_c} \cdot v'_z \cdot \partial \left[\frac{\mathrm{NO}]'}{\partial z = [\mathrm{NO}^0] \cdot D_{NO} \cdot \left[\nabla'^2 [\mathrm{NO}]'\right] - R_{NO}}\right. \tag{22}$$

$$R_{NO} = k_{ox,NO\text{-}RBC} \cdot \left[\mathrm{NO}\right]' \cdot [\mathrm{Hb}_{RBC}]_{\mathrm{total}} + k_{ox,NO\text{-}HBOC} \cdot \left[\mathrm{NO}\right]' \cdot [\mathrm{HBOC}]_{\mathrm{total}} \tag{23}$$

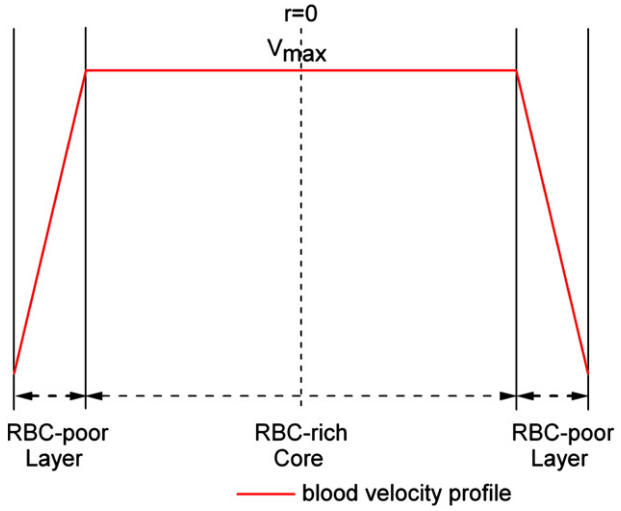

Fig. 2. Blood velocity profile in arteriole lumen [32,49].

3.2. Glycocalyx layer ($r_2<r\le r_3$)

The glycocalyx layer consists of a macromolecular mesh lining the surface of the luminal side of the endothelial cell layer [51], which is structurally composed of a complex network of polysaccharides and associated proteins such as albumin [52]. The thickness of the glycocalyx layer is estimated to be 0.5 μm [53]. As mentioned earlier, extravasation of Hb/HBOC through the blood vessel wall will be neglected in this model. Thus, O_2 and NO simply diffuse through this region without reaction. The steady-state transport of O_2 and NO is described by Eqs. (24) and (25).

$$0 = \alpha \cdot P_{50\text{-}RBC} \cdot D_{O2} \cdot \left[\nabla'^2 \left[\mathrm{pO_2}\right]'\right] \tag{24}$$

$$0 = [\mathrm{NO}]^0 \cdot D_{NO} \cdot \left[\nabla'^2 \left[\mathrm{NO}\right]'\right] \tag{25}$$

3.3. Endothelial cell layer ($r_3<r\le r_4$)

In the endothelial cell layer, the NO production rate was represented by R_{NO}' while the O_2 consumption rate was assumed to be twice the NO production rate [54,55] (Eq. (26)), while NO is generated proportional to the shear stress on the blood vessel wall in the range of 6–25 dyn/cm^2 [35] (Eqs. (27) and (28)), where Q is the

Table 1
Biophysical properties of PolyHbs and other HBOCs used in this study.

Solutions	P_{50} (mm Hg)	n	$k_{off,O2}$ (s^{-1})	$k_{ox,NO}$ ($\mu M^{-1}\,s^{-1}$)	Ref.
RBCs	29.3	2.2	4.4 [83]	0.14	[57,84]
20:1 L-PolyHb	37.1	1.05	58.6	17.1	[37]
20:1 H-PolyHb	2.18	0.6	29.7	16.4	[37]
30:1 L-PolyHb	41	1.01	57.1	18.7	[37]
30:1 H-PolyHb	1.84	0.69	24.7	17.5	[37]
40:1 H-PolyHb	0.66	0.57	22	17.5	[37]
50:1 L-PolyHb	41	0.87	53	18.9	[85]
Oxyglobin®	38	1.2	60	15	[86]
bHb	27	2.7	36.1	18	[37,87]

volumetric flow rate (ml/s) and η is the apparent solution viscosity. The blood vessel wall shear stress under normal physiological conditions consisting of blood velocity of 0.5 cm/s and apparent blood viscosity of 3.0 cP in an arteriole with a diameter of 50 μm was about 24 dyn/cm^2 [56] and is represented by *Shear_con*, while the shear stress upon transfusion of HBOCs is represented by *Shear_Exp*.

$$R_{O2} = -2\cdot R'_{NO} \tag{26}$$

$$R'_{NO} = R_{NO,control}\cdot\frac{Shear\_Exp}{Shear\_con} \tag{27}$$

$$Shear\_exp = \frac{4\cdot\eta\cdot Q}{\pi\cdot r_2^{\,3}} \tag{28}$$

The basal release rate of NO is assumed to be $5.3*10^{-12}$ mol*cm^{-2} s^{-1} at a normal blood vessel wall shear stress of 24 dyn/cm^2 under the action of a physiologically normal blood velocity of 0.5 cm/s and apparent blood viscosity of 3.0 cP in an arteriole with a diameter of 50 μm [56]. The endothelial layer in this chapter is assumed to have a thickness of 1 μm and length of 500 μm. Thus, the baseline NO release rate ($R_{NO,\ control}'$) is estimated to be 106 nM/s.

3.4. Interstitial layer ($r_4<r\le r_5$)

Similar to the glycocalyx layer, there is no Hb or RBCs present in the interstitial layer. O_2 and NO simply diffuse through this region and their steady-state transport is described by Eqs. (29) and (30).

$$0 = \alpha\cdot P_{50\text{-}RBC}\cdot D_{O2}\cdot\left[\nabla'^2[pO_2]'\right] \tag{29}$$

$$0 = [NO]^0\cdot D_{NO}\cdot\left[\nabla'^2[NO]'\right] \tag{30}$$

3.5. Smooth muscle cell layer ($r_5<r\le r_6$)

O_2 and NO diffuse into the smooth muscle cell layer and are consumed by the smooth muscle cells. The consumption of O_2 by smooth muscle cells is controlled by Michaelis–Menten (M–M) kinetics and inhibited in the presence of NO (Eq. (31)), where $Q_{max,sm}$ is the maximum O_2 consumption rate constant and K_{sm} is the M–M kinetic constant without NO present. The steady-state consumption of NO by the smooth muscle cells follows first-order kinetics (Eq. (32)) with $k_{NO\text{-}sm}$ as the first order NO reaction rate constant.

$$0 = \alpha\cdot P_{50\text{-}RBC}\cdot D_{O2}\cdot\left[\nabla'^2[pO_2]'\right] - Q_{max,sm}\cdot\frac{[pO_2]}{[pO_2]' + \left(K_{sm}\cdot\left(\frac{1+[NO]'}{0.027\,\mu M}\right)\right)} \tag{31}$$

$$0 = \left[NO^0\right]\cdot DNO\cdot\left[\nabla'^2[NO]'\right] - kNO\text{-}sm\cdot[NO]' \tag{32}$$

3.6. Tissue space ($r_6<r\le r_7$)

In the tissue space, O_2 and NO are transported by diffusion and are consumed by the tissue cells. Similarly, the consumption of O_2 in the tissue space follows M–M kinetics and is inhibited by the presence of NO (Eq. (33)), where $Q_{max,ts}$ is the maximum O_2 consumption rate constant in the tissue space and K_{ts} is the M–M kinetic constant in the tissue space in the absence of NO. The consumption of NO in the tissue space follows first-order kinetics (Eq. (34)), where $k_{NO\text{-}ts}$ is the first order NO reaction rate constant.

$$0 = \alpha\cdot P_{50\text{-}RBC}\cdot D_{O2}\cdot\left[\nabla'^2[pO_2]'\right] - Q_{max,ts}\cdot\frac{[pO_2]'}{[pO_2]' + \left(K_{ts}\cdot\left(\frac{1+[NO]'}{0.027\,\mu M}\right)\right)} \tag{33}$$

$$0 = [NO]^0\cdot D_{NO}\cdot\left[\nabla'^2[NO]'\right] - k_{NO\text{-}ts}\cdot[NO]' \tag{34}$$

3.6.1. Biophysical properties of PolyHbs used in this model

Two distinct types of PolyHb solutions, *i.e.* low O_2 affinity PolyHb (L-PolyHb) and high O_2 affinity PolyHb (H-PolyHb), which were synthesized with varying molar ratios of glutaraldehyde (cross-linker) to bHb (G:Hb) ranging from 20:1 to 50:1 [36,37], were evaluated in this model. The biophysical properties of PolyHbs and RBCs used in this work are listed in Tables 1 and 2. The diffusivities of PolyHbs and other HBOCs were calculated using Eq. (35), while the diffusivity of Hb encapsulated within RBCs was estimated using Eq. (36) [57]. We compared our results to simulations performed with the commercially available PolyHb Oxyglobin® and cell-free bHb.

$$D = 1.013\times10^{-4}(MW)^{-0.46}\left(cm^2/s\right) \tag{35}$$

Table 2
Diffusivity and Adair constants of PolyHbs and other HBOCs used in this study.

Solutions	Diffusivity (cm^2/s)	Adair parameters[a]				Ref.
		a_1	a_2	a_3	a_4	
RBCs	f(Hb)	$2.59*10^{-3}$	$1.77*10^{-3}$	$1.86*10^{-11}$	$1.39*10^{-6}$	[41]
20:1 L-PolyHb	$2.01*10^{-7}$[b]	$1.03*10^{-1}$	$4.21*10^{-3}$	$7.52*10^{-5}$	$5.27*10^{-7}$	b
20:1 H-PolyHb	$1.74*10^{-7}$[b]	14.139	7.7835	2.753	$4.17*10^{-2}$	
30:1 L-PolyHb	$1.54*10^{-7}$[b]	$9.73*10^{-2}$	$3.43*10^{-3}$	$5.41*10^{-5}$	$3.1*10^{-7}$	
30:1 H-PolyHb	$7.57*10^{-8}$[b]	8.2511	7.5548	6.4383	$5.98*10^{-1}$	
40:1 H-PolyHb	$3.91*10^{-8}$[b]	9.0158	24.717	27.613	1.1931	
50:1 L-PolyHb	$4.84*10^{-8}$[b]	$1.47*10^{-1}$	$5.20*10^{-3}$	$8.48*10^{-5}$	$3.40*10^{-7}$	
Oxyglobin®	$3.69*10^{-7}$[b]	$3.39*10^{-2}$	$2.49*10^{-3}$	$2.79*10^{-5}$	$6.55*10^{-7}$	[86]
bHb	$6.21*10^{-7}$[b]	$6.98*10^{-3}$	$2.15*10^{-3}$	$5.00*10^{-6}$	$1.88*10^{-6}$	[86]

[a] Adair parameters were curve fitted from O_2-HBOC equilibrium curves given in references [37,85] using the Adair equation.
[b] HBOC diffusivity was calculated using Eq. (35).

$$D_{Hb} = 9.74 * 10^{-7} * \left(1 - \frac{[\mathrm{Hb}]_{RBC} * hct}{46}\right) * 10^{-[\mathrm{Hb}]_{RBC} * hct / 128} \quad (36)$$

3.6.2. Model parameters

The constants and parameters used in this model are listed in Table 3. The arteriole diameter, average blood velocity and discharge *hct* (H_D) for these simulations were taken from experimental data reported in reference [39] and personal communications from Dr. Cabrales (Bioengineering Department) at the University of California, San Diego (UCSD): the H_D was set to 11% to mimic animal studies conducted using 50:1 L-PolyHb and 40:1 H-PolyHb solutions, while the H_D was set to 18% to mimic animal studies conducted using 20:1 and 30:1 L- and H-PolyHb solutions. The radius of the RBC-rich region (r_1) changes proportionally with the H_D [58,59], and the r_1 value used in this work was extrapolated from values of r_1 measured at *hct*s of 20%, 30% and 40% that were obtained from the literature [59]. For the calculation of NO transport, an inlet pO_2 of 60 mm Hg was chosen to mimic the inlet pO_2s reported in the literature [39]. For the simulation of O_2 transport facilitated by HBOCs, inlet pO_2 values were varied from 10 to 150 mm Hg to simulate both hypoxic and normal physiological conditions. The diffusivities of O_2 (D_{O2}) and NO (D_{NO}) in the solid phase (*i.e.* endothelial cell layer, smooth muscle cell layer and tissue space) were reported to be half of the values reported in free solution [60,61]. Thus in this work, D_{O2} and D_{NO} in these regions were assumed to be half of the values reported in blood phase. The overall concentration of HBOCs used in these simulations was estimated from animal studies described in the literature [39].

The viscosity of blood after transfusion with PolyHbs and other HBOCs was taken from reference [39] and personally communicated experimental results from Dr. Cabrales. The blood vessel wall shear stress upon transfusion of 20:1 and 30:1 PolyHbs was calculated using Eq. (28) and listed in Table 4, while the blood vessel wall shear stresses upon transfusion of 40:1 H and 50:1 L PolyHb solutions were taken from the experimental results contained in reference [39]. The viscosity of blood at *hct*s of 11% and 18% was estimated from the literature [62]. The effect of transfusion of Oxyglobin® and bHb on the resultant viscosity of blood was neglected in this study, since Oxyglobin® and bHb possess viscosities of 1.8 [39] and 1.6 [37] cP, respectively, even at concentrations higher than 10 g/dL.

Table 4
Blood viscosity and blood vessel wall shear stress after transfusion of PolyHb solutions.

Solution	Blood viscosity (cP)	Wall shear stress (dyn/cm^2)
11% hct	1.5	8.4
18% hct	1.9	10.9
20:1 L-PolyHb	4.1[a]	23.3
20:1 H-PolyHb	3.8[a]	21.6
30:1 L-PolyHb	4.6[a]	26.2
30:1 H-PolyHb	4.4[a]	25.1
40:1 H-PolyHb	2.5[39]	15.2[39]
50:1 L-PolyHb	2.9[39]	16.8[39]
Oxyglobin®	1.5 (11% *hct*)	8.4 (11% *hct*)
	1.9 (18% *hct*)	10.9 (18% *hct*)
bHb	1.5 (11% *hct*)	8.4 (11% *hct*)
	1.9 (18% *hct*)	10.9 (18% *hct*)

[a] Experimental results were obtained from Dr. Pedro Cabrales, Department of Bioengineering, University of California, San Diego.

4. Results

4.1. Effect of PolyHb on NO profiles

Vasoconstriction elicited by the transfusion of commercial HBOCs due to the undesired rapid scavenging of NO by HBOCs has long been considered one of the major side-effects hampering the clinical use of

Table 3
Constants and parameters used in the simulations.

Symbol	Simulation parameter	Value	Units	Ref
L_c	Length of arteriole	500	μm	[41]
R_c	Radius of arteriole	30	μm	[39]
U_{avg}	Average blood velocity	0.42	cm/s	[39]
$[\mathrm{Hb}]_{RBC}$	Concentration of Hb inside RBC	34	g/dL	[41]
$[\mathrm{Hb}]_{RBC\text{-}overall}$	Overall molar concentration of Hb in RBC: [heme]	21,250	μM	[29]
$[\mathrm{Hb}_{RBC}]_{total}/[HBOC]_{total}$	Local molar concentration of Hb in RBC or HBOC	Calculated from Eqs. (16) and (17)	μM	
H_D	Discharge *hct*	11% [39] and 18%[a]		[39]
H_C	*Hct* of RBC-rich core	0.13 for H_D 11% 0.20 for H_D 18%		Calculated from Eqs. (4)–(17)
$[NO]^0$	Basal NO concentration	0.01	μM	[41]
αO_2 (blood)	Solubility of O_2 in blood vessel	1.34	μmol/(L*mm Hg)	[49]
αO_2 (glycocalyx)	Solubility of O_2 in glycocalyx	1.34	μmol/(L*mm Hg)	[49]
αO_2 (endothelial)	Solubility of O_2 in endothelial cell layer	1.34	μmol/(L*mm Hg)	[49]
αO_2 (interstitial)	Solubility of O_2 in interstitial layer	1.10	μmol/(L*mm Hg)	[57]
αO_2 (smooth)	Solubility of O_2 in smooth muscle cell layer	1.34	μmol/(L*mm Hg)	[49]
αO_2 (tissue)	Solubility of O_2 in tissue	1.52	μmol/(L*mm Hg)	[49]
r_1	Radius of RBC-rich core	17.7 (H_D 11%) 19.8 (H_D 18%)	μm	Extrapolated from Ref. [59]
r_2	Outer radius of RBC-poor region	29.5	μm	[49]
r_3	Outer radius of glycocalyx	30	μm	[49]
r_4	Outer radius of endothelial cell layer	31	μm	[49]
r_5	Outer radius of interstitial layer	31.5	μm	[49]
r_6	Outer radius of smooth muscle cell layer	37.5	μm	[49]
r_7	Outer radius of tissue	135	μm	[49]
D_{O2}	Diffusivity of O_2	0.000028 or 0.000014	cm^2/s	[49,88]
D_{NO}	Diffusivity of NO	0.000033 or 0.0000165	cm^2/s	[49,88]
$[HBOC]_{overall}$	Overall concentration of PolyHb *in vivo*	3.5 or 10	g/dL	[39]
$Q_{max,sm}$	Maximum O_2 consumption rate constant in smooth muscle cell layer	1	μM/s	[49]
K_{sm}	M–M constant of O_2 consumption in smooth muscle cell layer	1	mm Hg	[49]
$k_{NO\text{-}sm}$	First order NO reaction rate constant in smooth muscle cell layer	0.05	1/(μM*s)	[12,84]
$Q_{max,ts}$	Maximum O_2 consumption rate constant in tissue	20	μM/s	[49]
K_{ts}	M–M constant of O_2 consumption in tissue	1	mm Hg	[49]
$k_{NO\text{-}ts}$	First order NO reaction rate constant in tissue	0.05	1/(μM*s)	[12,84]

[a] Personal communication from Dr. Pedro Cabrales, Department of Bioengineering, University of California, San Diego, CA.

HBOCs in transfusion medicine [8–10,63–65]. However, it has been demonstrated experimentally that transfusion of ultrahigh MW PolyHb solutions with high viscosity into animals exhibited less vasoactivity upon transfusion compared to the commercial PolyHb Oxyglobin® [38,39]. This is partly because administration of high viscosity solutions increases blood vessel wall shear stress, which induces the endothelium to produce the vasodilator NO [28,66–70] so as to offset the intrinsic NO scavenging effect of HBOCs. Thus in this work, we are also going to study the NO generating effect obtained via transfusion of high viscosity PolyHb solutions by computer simulation. In order to compare our results with 35% exchange transfusion experiments that were reported in the literature [39], the overall PolyHb concentration in our calculations was set to 3.5 g/dL and the inlet pO_2 was set to 60 mm Hg.

The effect of increasing blood vessel wall shear stress due to transfusion of high viscosity PolyHb solutions on the steady-state radial NO concentration profiles at *hct*s of 11% and 18% is shown in Fig. 3 and compared to radial NO concentration profiles without considering the influence of blood vessel wall shear stress-induced NO production. Hemodiluted blood at a *hct* of 11% [39] and 18% in the absence of HBOCs was used as controls. The radial NO concentration profiles displayed in Fig. 3 represent the NO concentration distribution at the axial midpoint of the arteriole ($Z = 250$ μm) and at an inlet $pO_2 = 60$ mm Hg. These results indicate that although the simulated steady-state radial NO concentration profiles upon transfusion of PolyHb solutions were very low inside arteriole lumen region (<0.2 nM) and lower than that of the control at both *hct*s, the NO-inducing effect of blood vessel wall shear stress greatly increased the overall steady-state concentration of NO across the region spanning the endothelial cell layer to the surrounding tissue space compared to not considering the NO-inducing ability of blood vessel wall shear stress. In addition, the overall computed steady-state NO concentration profile upon transfusion of ultrahigh MW PolyHbs was much higher than that of either Oxyglobin® or cell-free bHb.

The average NO concentration in the smooth muscle layer of the control and PolyHb-transfusion groups was calculated and compared in Fig. 4. Similarly, the control groups had the highest average NO concentration at the two *hct*s with the NO concentration at a *hct* of 18% slightly higher than that at a *hct* of 11%, due to the higher wall shear stress at a *hct* of 18%. However, when considering the NO-inducing effect of blood viscosity, the average NO concentration of the PolyHb-transfusion groups reached 50% ($hct = 11\%$) and 70% ($hct = 18\%$) of the control group regardless of the P_{50} and n of the PolyHb, while the NO concentration of no-shear-stress PolyHb solutions, Oxyglobin® and cell-free bHb groups was only about 20–30% of the control groups, indicating that the NO-inducing effect due to the induction of higher blood vessel shear stress caused by the transfusion of high viscosity PolyHb solutions can offset the harmful NO scavenging effect of HBOCs. Similarly, the concentration of NO inside the endothelial cell layer reached 45–70% of the control (*i.e.* includes RBCs but no HBOC) upon transfusion of high viscosity PolyHb (Fig. 5). Fig. 6 shows the relationship between the blood vessel wall shear stress and the average NO concentration in the arteriole region (Fig. 6.A) and the endothelial cell layer (blood vessel wall region) (Fig. 6.B) for all HBOCs. In both regions, the average NO concentration increased with blood vessel wall shear stress in an almost linear fashion, regardless of the $k_{ox,NO}$ values.

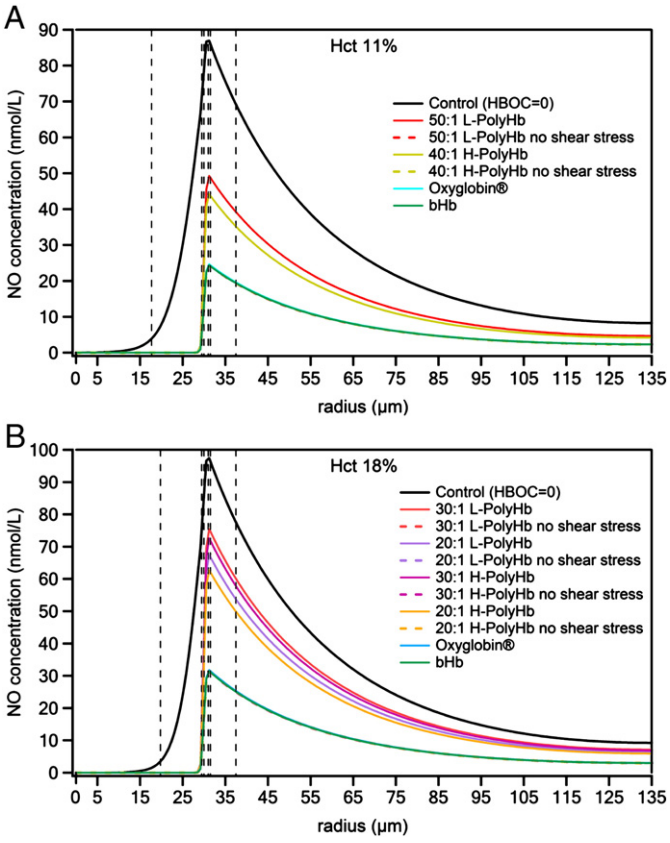

Fig. 3. The effect of increasing blood vessel wall shear stress upon transfusion of PolyHb solutions on the steady-state radial NO concentration profiles at an pO_2 inlet = 60 mm Hg: A: NO profile at hct = 11%; B: NO profile at hct = 18%. The vertical dashed lines represent the RBC-rich region, RBC-poor region, glycocalyx, endothelial cell layer, interstitial layer, smooth muscle cell layer and tissue space, respectively from left to right.

4.2. pO_2 profiles upon transfusion of Hb/PolyHb solutions

Figs. 7 and 8 display the steady-state radial O_2 tension profile under varying inlet pO_2s at the midpoint of the arteriole ($Z = 250$ μm) after transfusion of PolyHb solutions, with Oxyglobin® and cell-free bHb as negative controls for comparison. Diluted blood with a *hct* of 11% [39] and 18% in the absence of HBOC was used as a control. The inlet pO_2 levels were chosen to represent hypoxia (10 mm Hg), *in vivo* experimental conditions during hemodilution (60 mm Hg), normal physiological pO_2 in an arteriole before hemodilution (100 mm Hg) and room air levels of O_2 (150 mm Hg). The HBOC concentration used in the simulations was set to 3.5 g/dL [39] which was the overall HBOC concentration in a 35% exchange transfusion and 10 g/dL which is close to normal physiological Hb concentration [71]. NO production was assumed to be identical for both PolyHb concentrations. First at both *hct*s, transfusion of L-PolyHb solutions increased the *in vivo* oxygen tension from the arteriole lumen to the tissue space at all inlet pO_2 levels, in a dose-dependent manner especially in the RBC-poor region of the arteriole. In addition, transfusion of HBOCs increased the pO_2 profiles higher at a *hct* of 11% than at a *hct* of 18%, suggesting that L-PolyHb solutions could improve *in vivo* O_2 transport under conditions of serious blood loss. However, transfusion of too much PolyHb may cause an excessive rise in blood viscosity, which can cause a viscosity dependent rise in blood flow resistance and systemic hypertension [31]. Thus, more experiments should be conducted to optimize the concentration of L-PolyHb to be used in a clinical setting. Second, simulated pO_2 profiles are affected by the O_2 affinity of the PolyHb solution, which regulates the O_2 dissociation rate constant. All H-PolyHb solutions (P_{50}s ranging from 0.66 to 2 mm Hg) could improve O_2 transport to the tissue space to the same level as L-PolyHb solutions (P_{50}s ranging from 37 to 41 mm Hg), Oxyglobin® (P_{50} of 38 mm Hg) and cell-free bHb (P_{50} of 27 mm Hg) under hypoxic conditions (inlet $pO_2 = 10$ mm Hg) regardless of PolyHb molecular size and *hct*. However, H-PolyHbs exhibited less of an ability to improve O_2 transport than either L-PolyHb or Oxyglobin® at experimental hemodilution

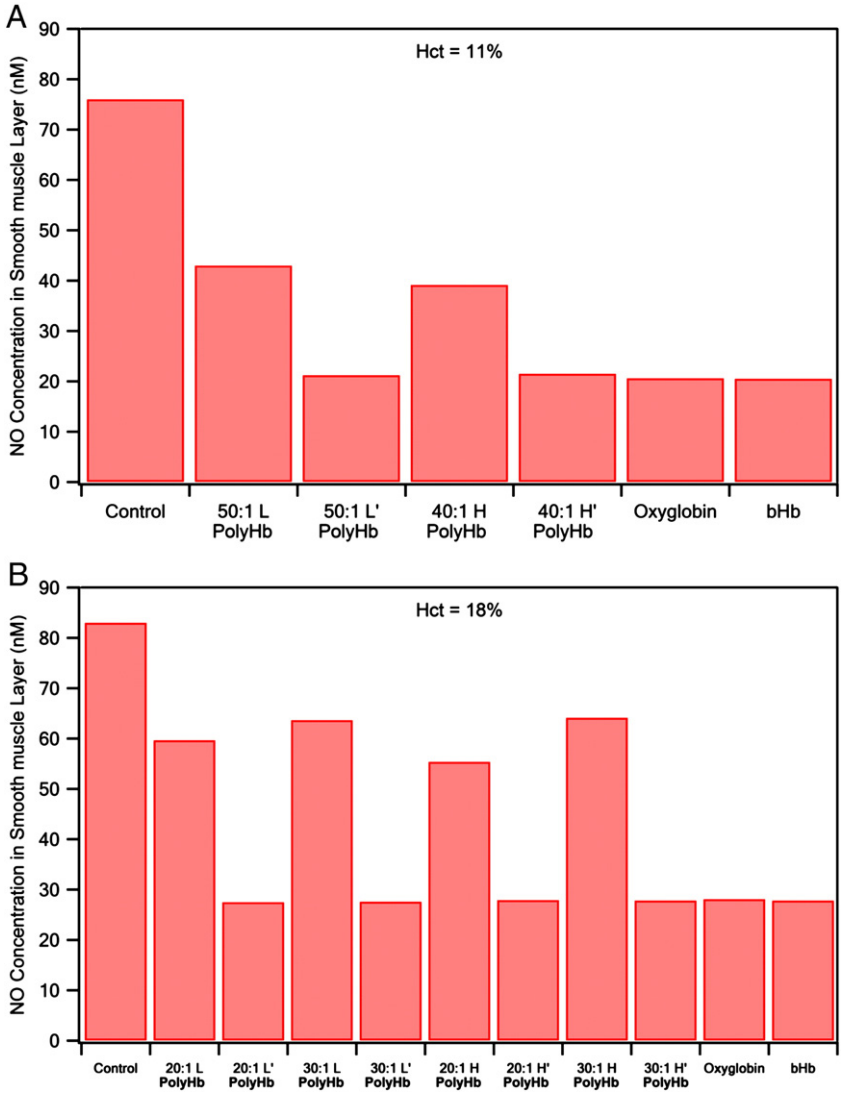

Fig. 4. The average NO concentration in the smooth muscle cell layer. A: Hct = 11%, L 50:1′ and H 40:1′ represent the groups that did not consider shear stress-induced production of NO by the endothelium; B: Hct = 18%, L 20:1′, L 30:1′ and H 20:1′, H 30:1′ represent the groups that did not consider shear stress-induced production of NO by the endothelium.

(60 mm Hg), normal physiological or supraphysiological (100 and 150 mm Hg) inlet pO_2 levels (Fig. 7B/C/D/F/G/H and Fig. 8B/C/D/F/G/H). In fact, increasing the O_2 affinity of H-PolyHb solutions reduced its ability to improve O_2 transport to the tissues upon transfusion. These results are in agreement with previous predictions in the literature [36,37], which showed that H-PolyHb solutions with extremely high O_2 affinity and low O_2 dissociation rate constant can potentially oxygenate hypoxic tissues, which is similar to that of MP4 [72,73], but is not effective at oxygenating tissues under normoxic conditions. In contrast, all L-PolyHb solutions possessed an enhanced ability to improve O_2 transport in the tissue space compared to H-PolyHb solutions and cell-free bHb and could increase the O_2 tension to a similar level as Oxyglobin® at all PolyHb concentrations and inlet pO_2s. These computer simulation results confirm the prediction that L-PolyHbs have the same O_2 transport ability as Oxyglobin®. In addition, cell-free bHb exhibited much less of an ability to improve O_2 transport than either L-PolyHb or Oxyglobin® at high inlet pO_2s (100–150 mm Hg, Fig. 7.D/G/H, Fig. 8.D/G/H) and was able to improve O_2 transport no better than 40:1 and 30:1 H-PolyHbs, which had the highest O_2 affinities among the HBOCs studied, at an inlet pO_2 of 150 mm Hg and at a *hct* of 18% especially at high HBOC concentrations (Figs. 7.H and 8.H). This phenomenon can be ascribed to two reasons. First, bHb possessed a lower O_2 dissociation rate constant (36.1 s^{-1}) compared to the PolyHbs (53–58 s^{-1}) and Oxyglobin® (60 s^{-1}). Second, because of the higher cooperativity (2.7) and O_2 association rate constant of bHb [37] compared to L-PolyHbs, bHb has a better chance of binding O_2 instead of releasing O_2 at high inlet pO_2s compared to L-PolyHbs.

4.3. O_2 transfer rate of PolyHbs

The O_2 transfer rates at steady-state after administration of HBOC solutions at varying inlet pO_2s from 10 to 150 mm Hg were calculated as the difference in the O_2 flux between the entrance and exit of the arteriole lumen and shown in Fig. 9 in comparison with those of Oxyglobin® and cell-free bHb. The O_2 transfer rates of RBCs in diluted blood at *hct*s of 11% and 18% were used as controls. At both *hct*s, the O_2 transfer rates of all simulation groups increased with increasing inlet pO_2 and reached a plateau when the inlet pO_2 was higher than 130 mm Hg. At a *hct* of 11% and at all inlet pO_2s (Fig. 9A), L- and H-PolyHbs exhibited higher calculated O_2 transfer rates than that of the control and any other HBOC. Interestingly, although H-PolyHb didn't enhance oxygenation of the tissue as effectively as L-PolyHb, 40:1 H-PolyHb had a slightly higher O_2 transfer rate than 50:1 L-

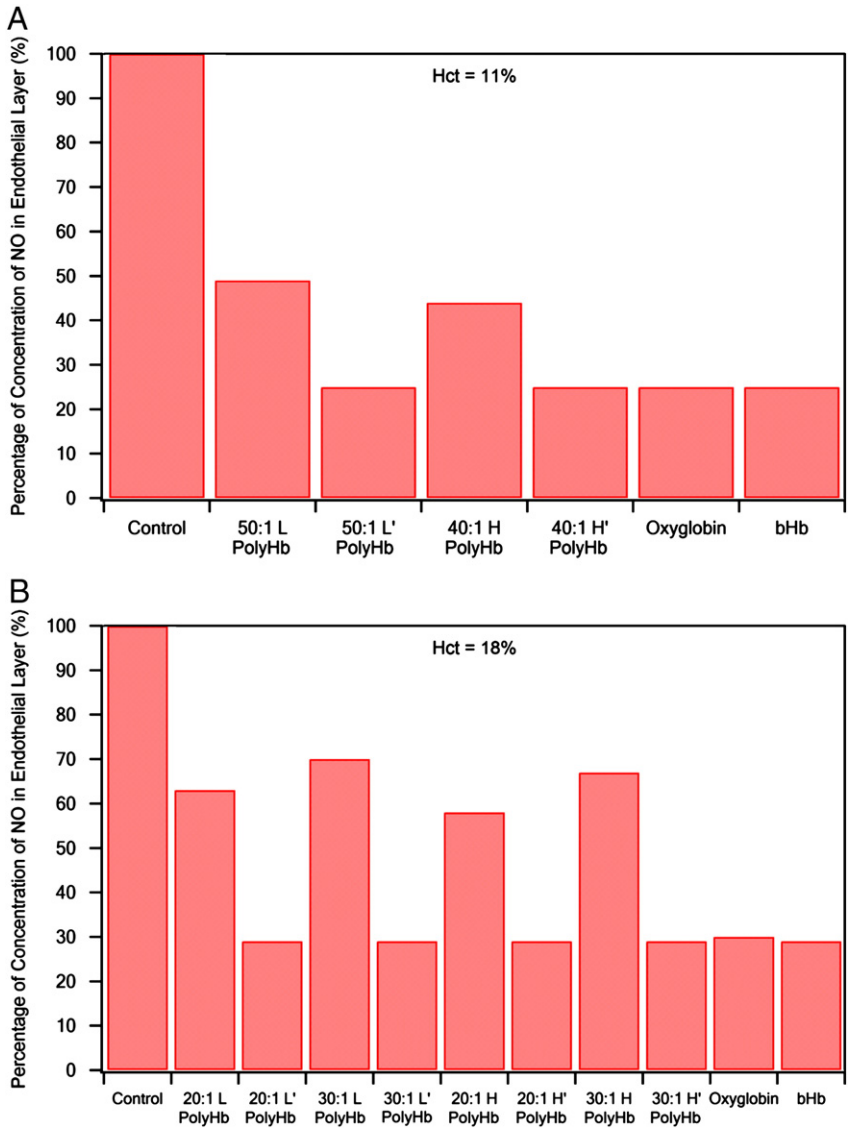

Fig. 5. The percentage average NO concentration inside the endothelial cell layer. A: Hct = 11%, L 50:1′ and H 40:1′ represent the groups that did not consider shear stress-induced production of NO by the endothelium; B: Hct = 18%, L 20:1′, L 30:1′, H 20:1′ and H 30:1′ represent the groups that did not consider shear stress-induced production of NO by the endothelium.

PolyHb at inlet pO_2s lower than 60 mm Hg, while L-PolyHb transferred O_2 faster at inlet pO_2s higher than 70 mm Hg. In contrast, Oxyglobin® and bHb had lower O_2 transfer rates than the control at inlet pO_2s lower than 70 mm Hg. When the inlet pO_2 was higher than 70 mm Hg, the O_2 transfer rates of Oxyglobin® and bHb rose to a similar level to that of H-PolyHb, which is consistent with the lower oxygenation ability of H-PolyHb. Similarly, at a *hct* of 18% (Fig. 9.B), two H-PolyHbs had similar O_2 transfer rates, which were higher than that of the control and any of the other HBOCs at low to medium inlet pO_2s (10–70 mm Hg). The O_2 transfer rates of both L-PolyHbs rose to a higher level than the control when the inlet pO_2 was higher than 60 mm Hg and to a similar level to H-PolyHb at an inlet pO_2 higher than 70 mm Hg. Again, the O_2 transfer rates of Oxyglobin® and bHb were the lowest when the inlet pO_2 was lower than 80 mm Hg and rose to a higher level compared to the control at an inlet pO_2 higher than 80 mm Hg. Interestingly, when the inlet pO_2 was lower than 70–80 mm Hg, the O_2 transfer rates were inversely related to the HBOC concentration at both *hct*s, while at an inlet pO_2 between 80 and 120 mm Hg, O_2 transfer rates increased with HBOC concentration at a *hct* of 11% but mainly remained unaffected by HBOC concentration at a *hct* of 18%.

5. Discussion

This work is aimed at predicting the effect of PolyHb's biophysical properties, for example O_2 affinity and viscosity, on the transport of NO and O_2 in an arteriole to primarily evaluate the efficacy and safety of PolyHbs in clinical applications via a mathematical model based on modification of the KTC model. An ideal HBOC should be able to improve tissue oxygenation, as well as, maintain adequate NO levels inside the smooth muscle layer to maintain vasodilation. In order to simulate the structure of an arteriole and blood flow, the physiological parameters of an arteriole such as *hct*, average blood velocity, diameter of arteriole lumen and blood viscosity after transfusion were all taken from *in vivo* experiments on PolyHb solutions [39]. The effect of endothelial-derived NO production induced by the high wall shear stress generated by the flow of high viscosity PolyHb solutions on NO transport was also investigated in this study.

In vivo, radial concentration profile of NO across the arteriole lumen to surrounding tissues should be determined by the balance of the NO scavenging rate of heme-containing macromolecules and the NO production rate of the endothelial cell layer. High viscosity PolyHb solutions tend to elevate blood and plasma viscosity in the

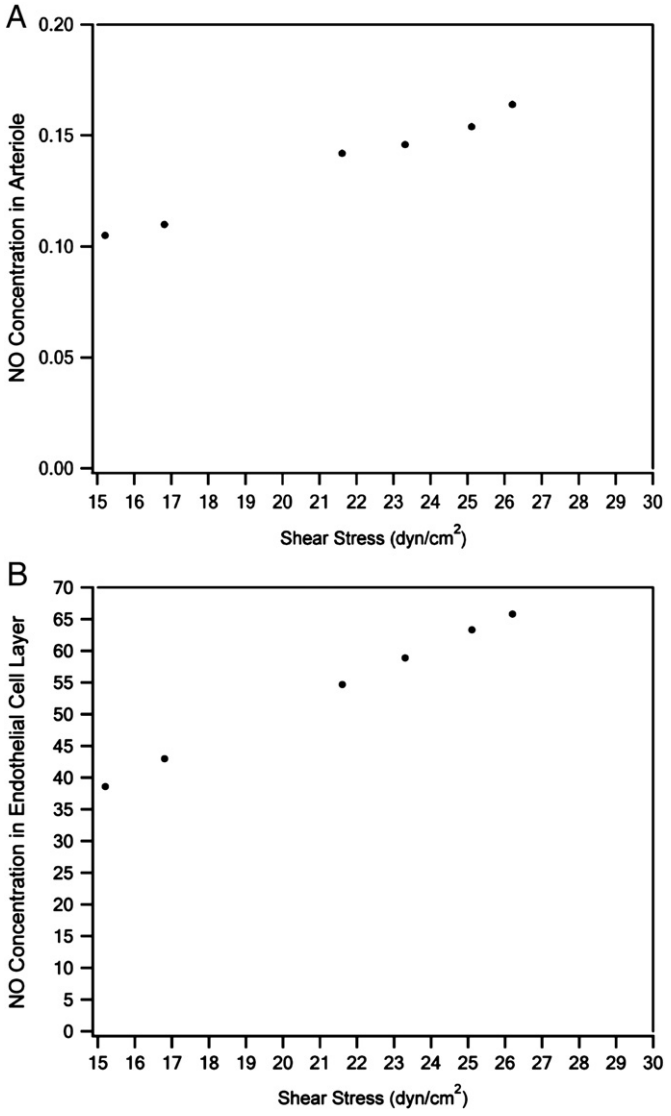

Fig. 6. The relationship between blood vessel wall shear stress and average NO concentration in the arteriole lumen (A) and the endothelial cell layer (B) for all PolyHb solutions.

systemic circulation, which was previously considered to be harmful, since blood viscosity was reported to be related to the physiopathology of hypertension and heart disease [30,74–77]. However, recent experiments and a mathematical model have demonstrated that slight elevation in blood viscosity, *e.g.* due to a slight increase in the *hct* by less than 19%, could lower the mean arterial pressure due to blood vessel wall shear stress-mediated production of the vasodilator NO [31,32,69]. The PolyHb solutions studied in this work increased the apparent blood viscosity after transfusion but didn't overly surpass the normal physiological blood viscosity (Table 4). Thus, transfusion of high viscosity PolyHb solutions is expected to increase the production of NO without excessively increasing blood flow resistance. On the other hand, all PolyHb solutions possess high NO dioxygenation rate constants compared to RBCs. Therefore, the NO concentration profile in the arteriole will be affected by the combined effects of the aforementioned two factors.

Table 5 lists the blood vessel wall shear stress reported in the literature with the calculated results using Eq. (28). It is evident that the calculated results are in good agreement with the experimental results. Thus, Eq. (28) was accurate in estimating the blood vessel wall shear stress for this simulation.

In our simulations, the two controls without HBOC had the highest radial NO concentration profiles across the arteriole into the tissue space at each respective *hct* (Figs. 3 to 5). Interestingly, the radial [NO] profiles and average NO concentrations of the two control groups in the arteriole lumen, endothelial cell layer and smooth muscle layer (Figs. 3 to 5) increased with increasing *hct*, although there were more RBCs present in the lumen of blood vessels at a *hct* of 18% to consume NO, indicating that when the NO consumption rate is low, enhancement in the NO production rate can offset the increased NO consumption by the increased *hct*. For PolyHbs, although their computationally calculated radial NO profiles were lower than those of the controls no matter whether the blood vessel wall shear stress was taken into account or not, the radial NO concentration profile upon transfusion of PolyHb solutions was observed to be much higher than that of Oxyglobin® and cell-free bHb. Transfusion of PolyHb solutions increased the NO release rate from the blood vessel wall 2–2.5 times compared to that of the control, since the NO production rate is linearly dependent on the blood vessel wall shear stress [34] within the physiological wall shear stress range of 6–25 dyn/cm^2 [35]. However, the NO dioxygenation rate constant ($k_{ox,NO}$) of PolyHbs and other HBOCs are two orders of magnitude higher than that of RBCs due to the presence of RBC membrane, which acts as a significant intracellular barrier against NO diffusion [78]. This explains why the radial NO concentration profiles of the controls were higher than that of the PolyHb solutions and other HBOCs with high NO dioxygenation rate constants. However, this result demonstrated that the enhanced NO production rate due to transfusion of high viscosity PolyHbs offsets the NO scavenging effect of the PolyHbs to a large extent. The calculated NO concentration upon transfusion of PolyHb solutions in the endothelial cell layer and smooth muscle layer was proportional to the blood vessel wall shear stress and could reach over 70% of the control values when the NO-inducing effect of high wall shear stress due to the high viscosity of PolyHb solutions was considered, while that of Oxyglobin® reached about 30% of the control ($\leq$27 nM). Condorelli and George reported that the median activation concentration of sGC in the smooth muscle layer by NO is approximately 23 nM [79]. Upon transfusion of PolyHb solutions, the simulated NO concentration inside the blood vessel wall ranged from 40 to 60 nM. Thus, transfusion of PolyHb solutions is expected to leave enough NO in the blood vessel wall for vasodilation compared to Oxyglobin®. This is consistent with published results of animal tests with high MW and high viscosity PolyHb solutions, in which a little to mild rise in mean arterial pressure was observed after transfusion of the >500 kDa fraction of ultrahigh MW PolyHb solutions [38,39], while transfusion of Oxyglobin® and PolyHb fractions smaller than 500 kDa with lower viscosity (1.0–1.4 cP) elicited a significant rise in mean arterial pressure [9,38,39]. Additionally, although it was expected that the extremely low diffusivities of PolyHbs in solution due to their ultrahigh MW could retard scavenging of NO by PolyHb in the arteriole lumen, simulation results showed that the NO concentration in the arteriole lumen upon transfusion of PolyHb was lower than 0.2 nM due to the high NO dioxygenation rate constant, which masked the effects of retarded diffusion of PolyHbs. In summary, according to our simulation results, the [NO] profile is primarily a function of the balance between the blood vessel wall shear stress-mediated NO production rate and the rate of NO scavenging. Another key result is that quenching of NO inside the arteriole lumen is unavoidable. However, it is possible to maintain adequate NO levels in the smooth muscle cell layer by increasing blood vessel wall shear stress. The blood vessel wall shear stress increases proportionally with the viscosity of blood, which depends on the concentration of PolyHb in the blood. However, an excessive increase in the viscosity of blood, *e.g.* higher than 50%, may offset the vasodilatory effect of shear stress-induced NO production via the viscosity dependent rise of blood flow resistance, which may cause hypertension [31]. Thus, more research

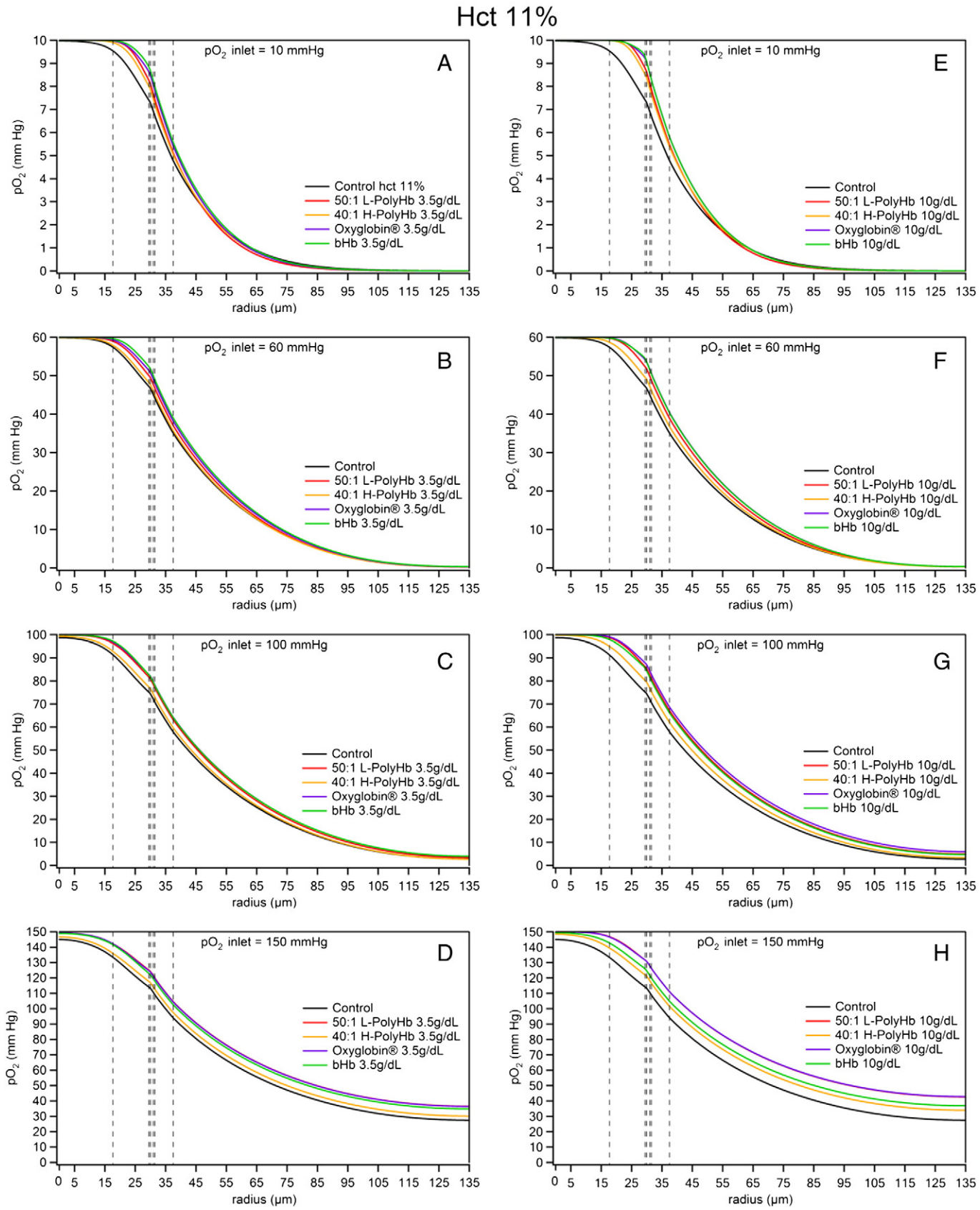

Fig. 7. Steady-state radial pO_2 profiles upon transfusion of PolyHb at *hct* = 11% and varying inlet pO_2s. A–D: PolyHb = 3.5 g/dL, inlet pO_2 = 10, 60, 100, 150 mm Hg; E–H: PolyHb = 10 g/dL, inlet pO_2 = 10, 60, 100, 150 mm Hg. The vertical dashed lines represent the RBC-rich region, RBC-poor region, glycocalyx, endothelial cell layer, interstitial layer, smooth muscle cell layer and tissue space, respectively from left to right.

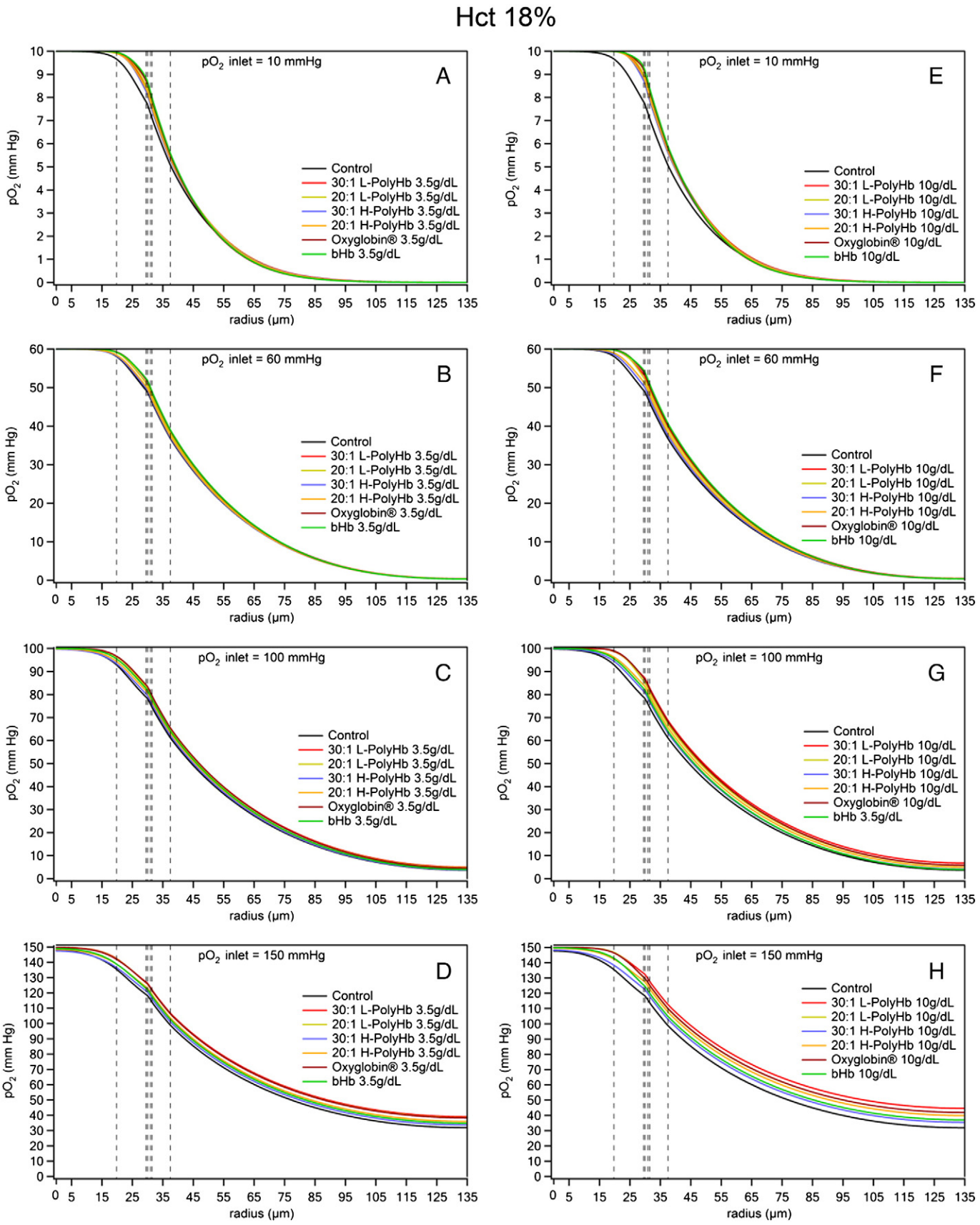

Fig. 8. Steady-state radial pO_2 profiles upon transfusion of PolyHb at *hct* = 18% and varying inlet pO_2s. A–D: PolyHb = 3.5 g/dL, inlet pO_2 = 10, 60, 100, 150 mm Hg; E–H: PolyHb = 10 g/dL, inlet pO_2 = 10, 60, 100, 150 mm Hg. The vertical dashed lines represent the RBC-rich region, RBC-poor region, glycocalyx, endothelial cell layer, interstitial layer, smooth muscle cell layer and tissue space, respectively from left to right.

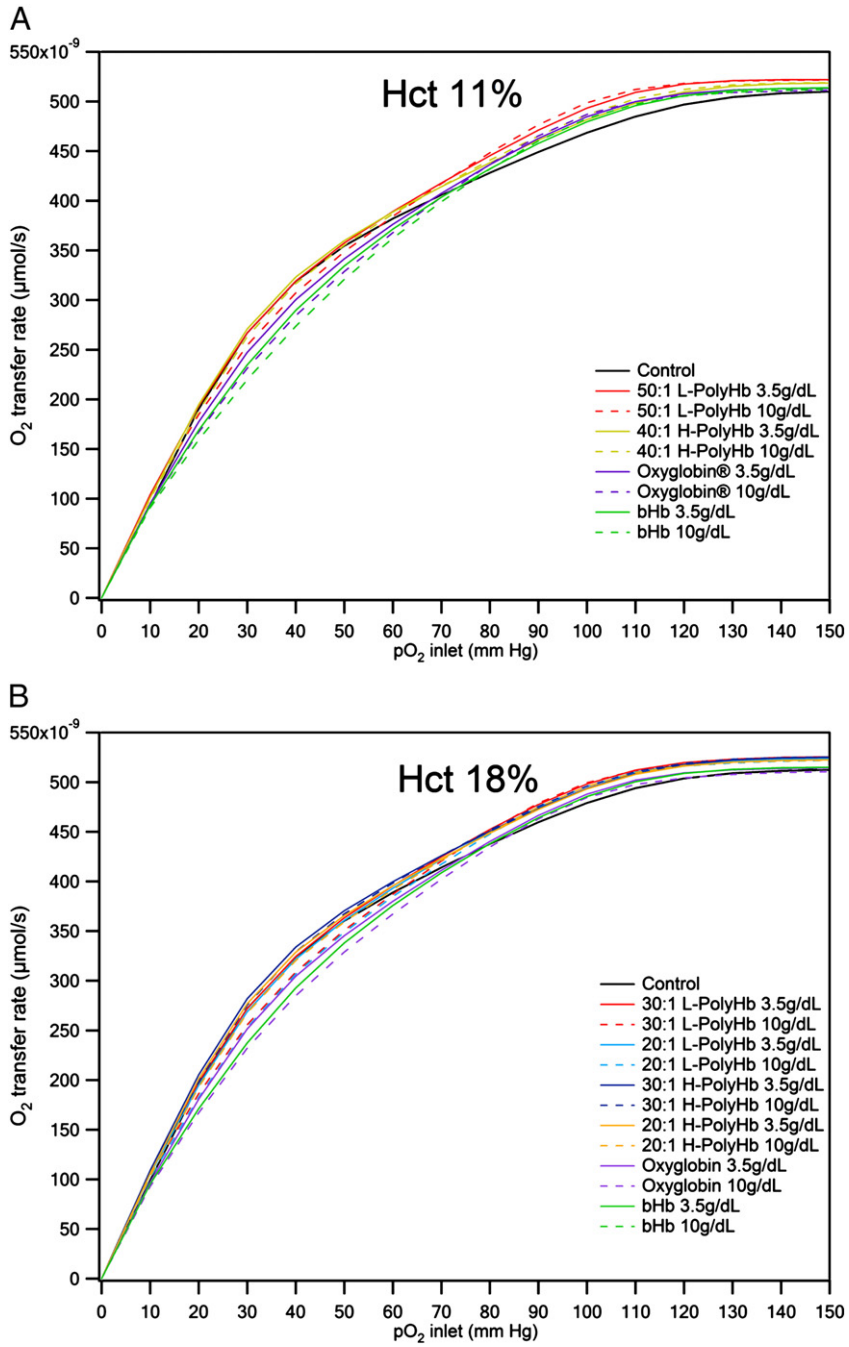

Fig. 9. O_2 transfer rate across the arteriole at different *hcts* and inlet pO_2s. A: O_2 transfer rate at a *hct* of 11% at [HBOC] = 3.5 g/dL and 10 g/dL, respectively. B: O_2 transfer rate at a *hct* of 18% at [HBOC] = 3.5 g/dL and 10 g/dL, respectively.

must be conducted to lower the intrinsic reactivity of PolyHb with NO, while maintaining the post-transfusion blood viscosity to 3–4 cP in order to induce blood vessel wall shear stress-dependent NO production. Additionally, the PolyHb concentration should also be optimized in order to not only maintain shear stress-induced NO production, but also to avoid viscosity-induced hypertension.

Table 5
Comparison of estimated blood vessel wall shear stress against experimentally measured blood vessel wall shear stress.

Blood sample	Calculated wall shear stress (dyn/cm^2)	Measured wall shear stress (dyn/cm^2)
Baseline (*hct* 48%)[39]	26.2	27.5[39]
Normal (*hct* 45%)[56]	23.9	24[56]
50:1 L-PolyHb	16.5	16.8[39]
40:1 H-PolyHb	14.2	15.2[39]

The radial pO_2 profiles are reported to be affected by the *hct* profile, blood velocity profile, radial distribution of HBOC and P_{50} [49]. Simulation results of the radial pO_2 distribution (Figs. 7 and 8) showed that transfusion of HBOC increased the pO_2 profiles most efficiently in the RBC-poor region of the arteriole at all inlet pO_2s and *hct*s. This is because HBOC molecules contribute a significant fraction of the total Hb concentration present in the RBC-poor region (Eq. (17)) due to the behavior of the paucity of RBC in this region. Thereby, more O_2 was released in this region than in the RBC-rich core. However, although the concentration of HBOC in the RBC-poor region increased with increasing r according to Eq. (17), the pO_2 dropped rapidly from the RBC-rich core to the glycocalyx layer

instead of increasing with HBOC concentration due to the rapid diffusion of O_2 into the neighboring endothelial cell layer where O_2 was rapidly consumed by these cells.

Comparing the simulation results using different HBOCs at varying concentrations and inlet pO_2s with *in vivo* measurements, all HBOCs only slightly improved oxygenation of the surrounding tissues, while either 50:1 L-PolyHb or 40:1 H-PolyHb could increase the average pO_2 in the arteriole by 30–60 mm Hg [39]. This discrepancy between simulation and experiments may be because in the model the HBOCs are assumed to be equilibrated with the inlet pO_2, while in the *in vivo* studies the PolyHb solutions, which were equilibrated with room air ($pO_2 \approx 144$ mm Hg), may contain large amounts of O_2 upon transfusion. Thus, the HBOC in the computer simulations can be much less O_2 saturated than those in the *in vivo* experiments, especially the L-PolyHbs, and the inlet concentration of O_2 carried by blood in the simulation can be much lower than that of the *in vivo* experiments, so that the amount of O_2 which can be offloaded to tissues may be underestimated in the simulations.

The O_2 affinity which is quantified by the P_{50} is another important factor that determines the efficacy of PolyHb solutions. Under hypoxic conditions (*e.g.* 10 mm Hg, Fig. 7.A/E and Fig. 8.A/E), H-PolyHb could obviously improve oxygenation of the surrounding tissues as efficiently as other HBOCs, while under normoxic conditions H-PolyHb hardly increases the pO_2 profile. The efficiency of tissue oxygenation displayed by high O_2 affinity PolyHb solutions in hypoxic regions is in agreement with results of previous simulations with low P_{50} HBOCs in a hepatic hollow fiber bioreactor [37]. Therefore, it is possible to use a mixture of L- and H-PolyHb for formulating the transfusion solution, in which H-PolyHb would oxygenate the extremely hypoxic tissues while L-PolyHb would oxygenate normoxic tissues. However, there is debate on the efficacy of low P_{50} HBOCs to oxygenate tissues under normoxic conditions. Sakai et al. [80] and Cabrales et al. [81] reported that transfusion of vesicle encapsulated Hb with high O_2 affinities oxygenated tissues better than vesicles with low O_2 affinities at an inlet pO_2 of 60 mm Hg. Tsai et al. [82] reported that MP4 ($P_{50} \approx 5$ mm Hg) could release more O_2 in the capillaries than Oxyglobin®. On the other hand, recently, Cabrales et al. [39] observed in animal tests that high O_2 affinity H-PolyHb was much less effective in oxygenating tissues surrounding arterioles than L-PolyHb. Our simulation results support the *in vivo* results obtained on transfusion of ultra-high MW PolyHbs. The discrepancy between our simulation results and *in vivo* results of transfusion of MP4 and Hb vesicles possessing high O_2 affinity may be caused by the different intrinsic biophysical properties of these HBOCs.

In contrast, all L-PolyHbs could obviously increase the *in vivo* pO_2 profiles to a similar level to that of Oxyglobin® at all inlet pO_2s (Figs. 7 and 8), irrespective of the cross-link density. The tissue oxygenation abilities of 20:1 and 30:1 PolyHbs were almost identical, which is consistent with their similar O_2 affinities and O_2 dissociation rate constants. However, the pO_2 profiles of cell-free bHb were slightly higher than those of L-PolyHbs at inlet pO_2s of 0 and 60 mm Hg at both *hct*s (Figs. 7A/B/E/F and 8), while the pO_2 profiles of Oxyglobin® were also higher than that of L-PolyHb at inlet pO_2s ranging from 10 to 100 mm Hg at a *hct* of 11% (Fig. 7.A/B/C/G/E/F, Fig. 8.A/B/C/G/E/F). This phenomenon is similar to O_2 transport simulation results obtained in hepatic hollow fiber bioreactors [37]. These results indicated that at low to medium *in vivo* pO_2s, the diffusion of HBOC molecules can have more of an influence on blood vessel and tissue oxygenation than the HBOC O_2 affinity and O_2 dissociation rate constant. Thus, confirming that the limited diffusion of PolyHb due to its ultrahigh MW may slightly retard offloading of O_2 to tissues. Therefore, these simulation results suggest that although high MW PolyHbs can help to eliminate the harmful extravasation of HBOC through the blood vessel wall and prolong the *in vivo* circulation time, the MW should be engineered to obtain optimum tissue oxygenation and the longest circulation time at all blood vessel inlet pO_2 levels.

Compared with the controls, Oxyglobin® and cell-free bHb, both L- and H-PolyHbs displayed higher O_2 transfer rates (Fig. 9). Patton and Palmer [57] predicted in a model of O_2 transport in a capillary that the release of O_2 from RBCs and HBOCs is affected by the HBOC/RBC O_2 affinity, cooperativity and HBOCs can compete with RBCs for O_2 and behave as sink for O_2 depending on the relative O_2 saturation of the RBCs and HBOCs. Our simulation results showed that the O_2 consumption rate, which was affected by the NO production rate, played a more important role in regulating the rate of O_2 delivery. For example, bHb has a higher O_2 saturation than L-PolyHb and Oxyglobin® at any pO_2, but lower O_2 transfer rate than those HBOCs under low to medium inlet pO_2s. In our simulations, Oxyglobin® and bHb had a lower O_2 transfer rate than the control and PolyHbs at inlet pO_2s ranging from 20 to 60 mm Hg. In this low inlet pO_2 range, HBOCs were partially O_2 saturated. Patton and Palmer [57] suggested that when the tissue including the endothelial cell layer, smooth muscle cell layer and surrounding tissue had low O_2 consumption, unconsumed O_2 could diffuse back into the arteriole lumen and bind to any heme-containing molecules with available O_2 binding sites. In our simulations, the NO production rate determines the O_2 consumption rate in the endothelium (Eq. (26)). Thus, Oxyglobin® and bHb possessed lower O_2 consumption rates compared to PolyHbs and behaved more like an O_2 sink. Cell-free bHb exhibited this O_2 sink effect more than Oxyglobin® in this inlet pO_2 range, since its higher cooperativity (2.7) and O_2 association rate constant which increases with increasing pO_2 made bHb more readily able to bind O_2. The O_2 "sink" effect of these HBOCs can be more pronounced at higher HBOC concentrations when more HBOC is available to bind O_2. When the inlet pO_2 was higher than 70 mm Hg, the O_2 "sink" effect of the HBOCs started to be gradually counteracted by the increasing amount of transported O_2 and the high O_2 dissociation rate constants of these HBOCs. Therefore, the HBOC's O_2 transfer rates increased significantly and surpassed that of the control, when the inlet pO_2 was higher than 70 mm Hg. On the other hand, O_2 diffusion from the plasma layer to the blood vessel wall could be improved 2–2.5 fold after transfusion of L- and H-PolyHbs compared to transfusion of other HBOCs due to the high NO production rate in the endothelial cell layer, which also increased the release of O_2 from PolyHbs regardless of their O_2 affinity and saturation. Therefore, PolyHbs displayed higher O_2 transfer rates compared to the control and the commercial HBOC Oxyglobin® or bHb.

6. Conclusions

NO and O_2 transport in an arteriole in the presence of RBCs and HBOCs under anemic conditions were studied in this work with a mathematical model. According to the simulation results, administration of high viscosity ultrahigh MW PolyHb solutions should yield less vasoconstriction by promoting blood vessel wall shear stress-dependent generation of the vasodilator NO, especially in the blood vessel walls compared to the commercial PolyHb Oxyglobin®. However, quenching of NO by PolyHb molecules in the arteriole lumen is inevitable due to the high NO dioxygenation rate constant of the PolyHb molecules. Under hypoxic conditions, all PolyHbs could improve tissue oxygenation under anemic conditions as effectively as the commercial HBOC Oxyglobin®, while L-PolyHb solutions were more effective in delivering O_2 than H-PolyHb solutions under normoxic conditions. In addition, all ultrahigh MW PolyHb displayed higher O_2 transfer rates than the commercial HBOC Oxyglobin®. Taken together, the simulation results indicate that a safe and efficacious HBOC should possess high viscosity and a low NO dioxygenation rate constant in order to reduce the side-effects associated with previous generations of acellular HBOCs.

Acknowledgments

This work was supported by National Institutes of Health grants R01HL078840 and R01DK070862 to AFP.

References

[1] J.Y. Chen, M. Scerbo, G. Kramer, A review of blood substitutes: examining the history, clinical trial results, and ethics of hemoglobin-based oxygen carriers, Clinics (São Paulo, Brazil) 64 (8) (2009) 803–813.
[2] A.G. Greenburg, The ideal blood substitute, Critical Care Clinics 25 (2) (2009) 415–424 Table of Contents.
[3] R.M. Winslow, Current status of oxygen carriers ('blood substitutes'): 2006, Vox Sanguinis 91 (2) (2006) 102–110.
[4] R.M. Winslow, Red cell substitutes, Seminars in Hematology 44 (1) (2007) 51–59.
[5] J.H. Lewis, Deantigenated beef blood plasma as a possible substitute for human blood plasma, Science (New York, NY) 98 (2547) (1943) 371–372.
[6] J.S. Jahr, M. Moallempour, J.C. Lim, HBOC-201, hemoglobin glutamer-250 (bovine), Hemopure (R) (Biopure Corporation), Expert Opin Biol Th 8 (9) (2008) 1425–1433.
[7] D. Freilich, L.B. Pearce, A. Pitman, G. Greenburg, M. Berzins, L. Bebris, S. Ahlers, R. McCarron, HBOC-201 vasoactivity in a phase III clinical trial in orthopedic surgery subjects—extrapolation of potential risk for acute trauma trials, The Journal of Trauma 66 (2) (2009) 365–376.
[8] C. Natanson, S.J. Kern, P. Lurie, S.M. Banks, S.M. Wolfe, Cell-free hemoglobin-based blood substitutes and risk of myocardial infarction and death: a meta-analysis, JAMA 299 (19) (2008) 2304–2312.
[9] J. Rice, N. Philbin, M. Handrigan, C. Hall, G. McGwin, S. Ahlers, L.B. Pearce, F. Arnaud, R. McCarron, D. Freilich, Vasoactivity of bovine polymerized hemoglobin (HBOC-201) in swine with traumatic hemorrhagic shock with and without brain injury, The Journal of Trauma 61 (5) (2006) 1085–1099.
[10] B. Yu, G.P. Volpato, K. Chang, K.D. Bloch, W.M. Zapol, Prevention of the pulmonary vasoconstrictor effects of HBOC-201 in awake lambs by continuously breathing nitric oxide, Anesthesiology 110 (1) (2009) 113–122.
[11] Q.H. Gibson, F.J.W. Roughton, The kinetics and equilibria of the reactions of nitric oxide with sheep haemoglobin, The Journal of Physiology 136 (3) (1957).
[12] M. Kavdia, N.M. Tsoukias, A.S. Popel, Model of nitric oxide diffusion in an arteriole: impact of hemoglobin-based blood substitutes, American Journal of Physiology — Heart and Circulatory Physiology 282 (6) (2002) H2245–H2253.
[13] G.C. Brown, V. Borutaite, Nitric oxide and mitochondrial respiration in the heart, Cardiovascular Research 75 (2) (2007) 283–290.
[14] S.A. Lipton, Physiology. Nitric oxide and respiration, Nature 413 (6852) (2001) 118–119 121.
[15] S. Moncada, E.A. Higgs, Nitric oxide and the vascular endothelium, Handbook of experimental pharmacology, 176, Pt 1, 2006, pp. 213–254.
[16] M. Ziche, Role of NO in angiogenesis, Journal of Vascular Research 41 (1) (2004) 95–95.
[17] M. Ziche, L. Morbidelli, Molecular regulation of tumour angiogenesis by nitric oxide, European Cytokine Network 20 (4) (2009) 164–170.
[18] R.B. Weller, Nitric oxide-containing nanoparticles as an antimicrobial agent and enhancer of wound healing, The Journal of Investigative Dermatology 129 (10) (2009) 2335–2337.
[19] H. Zhu, X. Wei, K. Bian, F. Murad, Effects of nitric oxide on skin burn wound healing, Journal of Burn Care & Research 29 (5) (2008) 804–814.
[20] S.R. Vincent, Nitric oxide neurons and neurotransmission, Progress in Neurobiology 90 (2) (2010) 246–255.
[21] K. Chen, R.N. Pittman, A.S. Popel, Nitric oxide in the vasculature: where does it come from and where does it go? A quantitative perspective, Antioxidants & Redox Signaling 10 (7) (2008) 1185–1198.
[22] R.F. Furchgott, M.H. Carvalho, M.T. Khan, K. Matsunaga, Evidence for endothelium-dependent vasodilation of resistance vessels by acetylcholine, Blood Vessels 24 (3) (1987) 145–149.
[23] L.J. Ignarro, G.M. Buga, K.S. Wood, R.E. Byrns, G. Chaudhuri, Endothelium-derived relaxing factor produced and released from artery and vein is nitric oxide, Proceedings of the National Academy of Sciences of the United States of America 84 (24) (1987) 9265–9269.
[24] J.W. Denninger, M.A. Marletta, Guanylate cyclase and the NO/cGMP signaling pathway, Biochimica et Biophysica Acta 1411 (2–3) (1999) 334–350.
[25] J.S. Olson, E.W. Foley, C. Rogge, A.L. Tsai, M.P. Doyle, D.D. Lemon, No scavenging and the hypertensive effect of hemoglobin-based blood substitutes, Free Radical Biology & Medicine 36 (6) (2004) 685–697.
[26] J.S. Olson, E.W. Foley, C. Rogge, A.L. Tsai, M.P. Doyle, D.D. Lemon, No scavenging and the hypertensive effect of hemoglobin-based blood substitutes, Free Radical Biology & Medicine 36 (6) (2004) 685–697.
[27] D.M. Dudzinski, J. Igarashi, D. Greif, T. Michel, The regulation and pharmacology of endothelial nitric oxide synthase, Annual Review of Pharmacology and Toxicology 46 (2006) 235–276.
[28] G.M. Buga, M.E. Gold, J.M. Fukuto, L.J. Ignarro, Shear stress-induced release of nitric oxide from endothelial cells grown on beads, Hypertension 17 (2) (1991) 187–193.
[29] J.L. Garvin, P.D. Cabral, N.J. Hong, Shear stress increases nitric oxide production in thick ascending limbs, Am J Physiol-Renal 299 (5) (2010) F1185–F1192.
[30] J. Martini, B. Carpentier, A.C. Negrete, P. Cabrales, A.G. Tsai, M. Intaglietta, Beneficial effects due to increasing blood and plasma viscosity, Clin Hemorheol Micro 35 (1–2) (2006) 51–57.
[31] J. Martini, B. Carpentier, A.C. Negrete, J.A. Frangos, M. Intaglietta, Paradoxical hypotension following increased hematocrit and blood viscosity, American Journal of Physiology — Heart and Circulatory Physiology 289 (5) (2005) H2136–H2143.
[32] K. Sriram, B.Y. Vazquez, O. Yalcin, P.C. Johnson, M. Intaglietta, D.M. Tartakovsky, The effect of small changes in hematocrit on nitric oxide transport in arterioles, Antioxid Redox Sign 14 (2) (2010) 175–185.
[33] P. Ulker, N. Yaras, O. Yalcin, C. Celik-Ozenci, P.C. Johnson, H.J. Meiselman, O.K. Baskurt, Shear stress activation of nitric oxide synthase and increased nitric oxide levels in human red blood cells, Nitric Oxide 24 (4) (2011) 184–191.
[34] A.J. Kanai, H.C. Strauss, G.A. Truskey, A.L. Crews, S. Grunfeld, T. Malinski, Shear stress induces ATP-independent transient nitric oxide release from vascular endothelial cells, measured directly with a porphyrinic microsensor, Circulation Research 77 (2) (1995) 284–293.
[35] M.J. Kuchan, J.A. Frangos, Role of calcium and calmodulin in flow-induced nitric-oxide production in endothelial-cells, American Journal of Physiology 266 (3) (1994) C628–C636.
[36] P.W. Buehler, Y. Zhou, P. Cabrales, Y. Jia, G. Sun, D.R. Harris, A.G. Tsai, M. Intaglietta, A.F. Palmer, Synthesis, biophysical properties and pharmacokinetics of ultrahigh molecular weight tense and relaxed state polymerized bovine hemoglobins, Biomaterials 31 (13) (2010) 3723–3735.
[37] Y.P. Zhou, Y.P. Jia, P.W. Buehler, G. Chen, P. Cabrales, A.F. Palmer, Synthesis, biophysical properties, and oxygenation potential of variable molecular weight glutaraldehyde-polymerized bovine hemoglobins with low and high oxygen affinity, Biotechnol Progr 27 (4) (2011) 1172–1184.
[38] P. Cabrales, G.Y. Sun, Y.P. Zhou, D.R. Harris, A.G. Tsai, M. Intaglietta, A.F. Palmer, Effects of the molecular mass of tense-state polymerized bovine hemoglobin on blood pressure and vasoconstriction, Journal of Applied Physiology 107 (5) (2009) 1548–1558.
[39] P. Cabrales, Y. Zhou, D.R. Harris, A.F. Palmer, Tissue oxygenation after exchange transfusion with ultrahigh-molecular-weight tense- and relaxed-state polymerized bovine hemoglobins, American Journal of Physiology — Heart and Circulatory Physiology 298 (3) (2010) H1062–H1071.
[40] B. Driessen, J.S. Jahr, F. Lurie, R.A. Gunther, Inadequacy of low-volume resuscitation with hemoglobin-based oxygen carrier hemoglobin glutamer-200 (bovine) in canine hypovolemia, Journal of Veterinary Pharmacology and Therapeutics 24 (1) (2001) 61–71.
[41] S.I. Gundersen, G. Chen, A.F. Palmer, Mathematical model of NO and O_2 transport in an arteriole facilitated by hemoglobin based O_2 carriers, Biophysical Chemistry 143 (1–2) (2009) 1–17.
[42] A.S. Popel, Theory of oxygen transport to tissue, Critical Reviews in Biomedical Engineering 17 (3) (1989) 257–321.
[43] G.S. Adair, The hemoglobin system. VI. The oxygen dissociation curve of hemoglobin, Journal of Biological Chemistry 63 (2) (1925) 529–545.
[44] A.V. Hill, The combinations of haemoglobin with oxygen and with carbon monoxide. I, The Biochemical Journal 7 (5) (1913) 471–480.
[45] J.P. Sullivan, J.E. Gordon, A.F. Palmer, Simulation of oxygen carrier mediated oxygen transport to C3A hepatoma cells housed within a hollow fiber bioreactor, Biotechnology and Bioengineering 93 (2) (2006) 306–317.
[46] A. Vander, J. Sherman, D. Luciano, Circulation, Vander's Human Physiology: The Mechanisms of Body Function, Eighth ed, McGraw-Hill, Boston, 2001, pp. 373–462.
[47] M. Sharan, A.S. Popel, A two-phase model for flow of blood in narrow tubes with increased effective viscosity near the wall, Biorheology 38 (5–6) (2001) 415–428.
[48] A.G. Tsai, P.C. Johnson, M. Intaglietta, Oxygen gradients in the microcirculation, Physiological Reviews 83 (3) (2003) 933–963.
[49] X. Chen, D. Jaron, K.A. Barbee, D.G. Buerk, The influence of radial RBC distribution, blood velocity profiles, and glycocalyx on coupled NO/O_2 transport, Journal of Applied Physiology 100 (2) (2006) 482–492.
[50] D.G. Buerk, Can we model nitric oxide biotransport? A survey of mathematical models for a simple diatomic molecule with surprisingly complex biological activities, Annual Review of Biomedical Engineering 3 (2001) 109–143.
[51] S. Weinbaum, J.M. Tarbell, E.R. Damiano, The structure and function of the endothelial glycocalyx layer, Annual Review of Biomedical Engineering 9 (2007) 121–167.
[52] H.A. Levine, M.P. McGee, S. Serna, Diffusion and reaction in the cell glycocalyx and the extracellular matrix, Journal of Mathematical Biology 60 (1) (2010) 1–26.
[53] B.M. van den Berg, H. Vink, J.A. Spaan, The endothelial glycocalyx protects against myocardial edema, Circulation Research 92 (6) (2003) 592–594.
[54] X. Chen, D.G. Buerk, K.A. Barbee, D. Jaron, A model of NO/O_2 transport in capillary-perfused tissue containing an arteriole and venule pair, Annals of Biomedical Engineering 35 (4) (2007) 517–529.
[55] K. Chen, A.S. Popel, Theoretical analysis of biochemical pathways of nitric oxide release from vascular endothelial cells, Free Radical Biology & Medicine 41 (4) (2006) 668–680.
[56] J.C. Liao, M.W. Vaughn, L. Kuo, Estimation of nitric oxide production and reaction rates in tissue by use of a mathematical model, Am J Physiol-Heart C 274 (6) (1998) H2163–H2176.
[57] J.N. Patton, A.F. Palmer, Numerical simulation of oxygen delivery to muscle tissue in the presence of hemoglobin-based oxygen carriers, Biotechnology Progress 22 (4) (2006) 1025–1049.
[58] R.H. Cole, K.D. Vandegriff, A.J. Szeri, O. Savas, D.A. Baker, R.M. Winslow, A quantitative framework for the design of acellular hemoglobins as blood substitutes: implications of dynamic flow conditions, Biophysical Chemistry 128 (1) (2007) 63–74.
[59] N. Tateishi, Y. Suzuki, I. Cicha, N. Maeda, O_2 release from erythrocytes flowing in a narrow O_2-permeable tube: effects of erythrocyte aggregation, American Journal of Physiology — Heart and Circulatory Physiology 281 (1) (2001) H448–H456.

[60] S. Fischkoff, J.M. Vanderkooi, Oxygen diffusion in biological and artificial membranes determined by the fluorochrome pyrene, The Journal of General Physiology 65 (5) (1975) 663–676.
[61] M. Mahler, C. Louy, E. Homsher, A. Peskoff, Reappraisal of diffusion, solubility, and consumption of oxygen in frog skeletal muscle, with applications to muscle energy balance, The Journal of General Physiology 86 (1) (1985) 105–134.
[62] G.K. Snyder, Influence of temperature and hematocrit on blood viscosity, The American Journal of Physiology 220 (6) (1971) 1667–1672.
[63] P.W. Buehler, A.I. Alayash, Toxicities of hemoglobin solutions: in search of in-vitro and in-vivo model systems, Transfusion 44 (10) (2004) 1516–1530.
[64] P.W. Buehler, F. D'Agnillo, Toxicological consequences of extracellular hemoglobin: biochemical and physiological perspectives, Antioxidants & Redox Signaling 12 (2) (2010) 275–291.
[65] J. Simoni, G. Simoni, J.F. Moeller, Intrinsic toxicity of hemoglobin: how to counteract it, Artificial Organs 33 (2) (2009) 100–109.
[66] F.M. Box, R.J. van der Geest, M.C. Rutten, J.H. Reiber, The influence of flow, vessel diameter, and non-Newtonian blood viscosity on the wall shear stress in a carotid bifurcation model for unsteady flow, Investigative Radiology 40 (5) (2005) 277–294.
[67] G.K. Kolluru, S. Sinha, S. Majumder, A. Muley, J.H. Siamwala, R. Gupta, S. Chatterjee, Shear stress promotes nitric oxide production in endothelial cells by sub-cellular delocalization of eNOS: a basis for shear stress mediated angiogenesis, Nitric Oxide 22 (4) (2010) 304–315.
[68] B. Sprague, N.C. Chesler, R.R. Magness, Shear stress regulation of nitric oxide production in uterine and placental artery endothelial cells: experimental studies and hemodynamic models of shear stresses on endothelial cells, International Journal of Developmental Biology 54 (2–3) (2010) 331–339.
[69] A.G. Tsai, C. Acero, P.R. Nance, P. Cabrales, J.A. Frangos, D.G. Buerk, M. Intaglietta, Elevated plasma viscosity in extreme hemodilution increases perivascular nitric oxide concentration and microvascular perfusion, American Journal of Physiology — Heart and Circulatory Physiology 288 (4) (2005) H1730–H1739.
[70] A.G. Tsai, M. Intaglietta, High viscosity plasma expanders: volume restitution fluids for lowering the transfusion trigger, Biorheology 38 (2–3) (2001) 229–237.
[71] I.C. Macdougall, Individualizing target haemoglobin concentrations — tailoring treatment for renal anaemia, Nephrology, Dialysis, Transplantation 16 (2001) 9–14.
[72] K.D. Vandegriff, A. Malavalli, J. Wooldridge, J. Lohman, R.M. Winslow, MP4, a new nonvasoactive PEG-Hb conjugate, Transfusion 43 (4) (2003) 509–516.
[73] R.M. Winslow, MP4, a new nonvasoactive polyethylene glycol-hemoglobin conjugate, Artificial Organs 28 (9) (2004) 800–806.
[74] R.S. Rosenson, S. Shott, C.C. Tangney, Elevated blood viscosity contributes to coronary heart disease risk in hypertriglyceridemia subjects, Atherosclerosis 134 (1–2) (1997) 94–94.
[75] R.B. Devereux, D.B. Case, M.H. Alderman, T.G. Pickering, S. Chien, J.H. Laragh, Possible role of increased blood viscosity in the hemodynamics of systemic hypertension, The American Journal of Cardiology 85 (10) (2000) 1265–+.
[76] S.M. Macrury, M. Small, A.C. Maccuish, G.D. Lowe, Association of hypertension with blood-viscosity in diabetes, Diabetic Medicine 5 (9) (1988) 830–834.
[77] R.L. Letcher, S. Chien, T.G. Pickering, J.E. Sealey, J.H. Laragh, Direct relationship between blood pressure and blood viscosity in normal and hypertensive subjects. Role of fibrinogen and concentration, The American Journal of Medicine 70 (6) (1981) 1195–1202.
[78] K.T. Huang, T.H. Han, D.R. Hyduke, M.W. Vaughn, H. Van Herle, T.W. Hein, C. Zhang, L. Kuo, J.C. Liao, Modulation of nitric oxide bioavailability by erythrocytes, Proceedings of the National Academy of Sciences of the United States of America 98 (20) (2001) 11771–11776.
[79] P. Condorelli, S.C. George, In vivo control of soluble guanylate cyclase activation by nitric oxide: a kinetic analysis, Biophysical Journal 80 (5) (2001) 2110–2119.
[80] H. Sakai, P. Cabrales, A.G. Tsai, E. Tsuchida, M. Intaglietta, Oxygen release from low and normal P50 Hb vesicles in transiently occluded arterioles of the hamster window model, American Journal of Physiology — Heart and Circulatory Physiology 288 (6) (2005) H2897–H2903.
[81] P. Cabrales, H. Sakai, A.G. Tsai, S. Takeoka, E. Tsuchida, M. Intaglietta, Oxygen transport by low and normal oxygen affinity hemoglobin vesicles in extreme hemodilution, American Journal of Physiology — Heart and Circulatory Physiology 288 (4) (2005) H1885–H1892.
[82] A.G. Tsai, K.D. Vandegriff, M. Intaglietta, R.M. Winslow, Targeted O_2 delivery by low-P50 hemoglobin: a new basis for O_2 therapeutics, American Journal of Physiology — Heart and Circulatory Physiology 285 (4) (2003) H1411–H1419.
[83] H. Sakai, A.G. Tsai, R.J. Rohlfs, H. Hara, S. Takeoka, E. Tsuchida, M. Intaglietta, Microvascular responses to hemodilution with Hb vesicles as red blood cell substitutes: influence of O_2 affinity, The American Journal of Physiology 276 (2 Pt 2) (1999) H553–H562.
[84] M. Kavdia, A.S. Popel, Wall shear stress differentially affects NO level in arterioles for volume expanders and Hb-based O_2 carriers, Microvascular Research 66 (1) (2003) 49–58.
[85] P.W. Buehler, Y. Zhou, P. Cabrales, Y. Jia, G. Sun, D.R. Harris, A.G. Tsai, M. Intaglietta, A.F. Palmer, Synthesis, biophysical properties and pharmacokinetics of ultrahigh molecular weight tense and relaxed state polymerized bovine hemoglobins, Biomaterials 31 (13) (2010) 3723–3735.
[86] P.W. Buehler, R.A. Boykins, Y.P. Jia, S. Norris, D.I. Freedberg, A.I. Alayash, Structural and functional characterization of glutaraldehyde-polymerized bovine hemoglobin and its isolated fractions, Analytical Chemistry 77 (11) (2005) 3466–3478.
[87] J. Elmer, P.W. Buehler, Y.P. Jia, F. Wood, D.R. Harris, A.I. Alayash, A.F. Palmer, Functional comparison of hemoglobin purified by different methods and their biophysical implications, Biotechnology and Bioengineering 106 (1) (2010) 76–85.
[88] M. Intaglietta, K. Sriram, B.Y.S. Vazquez, O. Yalcin, P.C. Johnson, D.M. Tartakovsky, The effect of small changes in hematocrit on nitric oxide transport in arterioles, Antioxidants & Redox Signaling 14 (2) (2011) 175–185.